Extremely strong-coupling superconductivity and anomalous lattice properties in the β-pyrochlore oxide KOs_2O_6

Z. Hiroi, S. Yonezawa, Y. Nagao and J. Yamaura
Institute for Solid State Physics, University of Tokyo, Kashiwa, Chiba 277-8581, Japan

Superconducting and normal-state properties of the β-pyrochlore oxide KOs_2O_6 are studied by means of thermodynamic and transport measurements. It is shown that the superconductivity is of conventional *s*-wave type and lies in the extremely strong-coupling regime. Specific heat and resistivity measurements reveal that there are characteristic low-energy phonons that give rise to unusual scattering of carriers due to strong electron-phonon interactions. The entity of the low-energy phonons is ascribed to the heavy rattling of the K ion confined in an oversized cage made of OsO_6 octahedra. It is suggested that this electron-rattler coupling mediates the Cooper pairing, resulting in the extremely strong-coupling superconductivity.

I. INTRODUCTION

The study of non-Cu-based oxide superconductors has been extended during the last decade, aiming at understanding the role of electron correlations in the mechanism of superconductivity or searching for a novel pairing mechanism, hopefully to reach a higher T_c. An interesting example recently found is a family of pyrochlore oxide superconductors. The first discovered is α-pyrochlore rhenate $Cd_2Re_2O_7$ with T_c = 1.0 K[1-3] and the second β-pyrochlore osmate AOs_2O_6 with T_c = 3.3, 6.3, and 9.6 K for A = Cs,[4] Rb,[5-7] and K,[8] respectively. They crystallize in the cubic pyrochlore structure of space group Fd-3m and commonly possess a 3D skeleton made of ReO_6 or OsO_6 octahedra.[9] The "pyrochlore" sublattice occupied by the transition metal ions is comprised of corner-sharing tetrahedra that are known to be highly frustrating for a localized spin system with antiferromagnetic nearest-neighbor interactions.

A unique structural feature for the β-pyrochlores is that a relatively small A ion is located in an oversized atomic cage made of OsO_6 octahedra, Fig. 1. Due to this large size mismatch, the A atom can rattle in the cage.[10] The rattling has been recognized recently as an interesting phenomenon for a class of compounds like filled skutterudites[11] and Ge/Si clathrates[12] and attracted many researchers, because it may suppress thermal conductivity leading to an enhanced thermoelectric efficiency. On the other hand, the rattling is also intriguing from the viewpoint of lattice dynamics: it gives an almost localized mode even in a crystalline material and often exhibits unusual anharmonicity.[11] Hence, it is considered that the rattling is a new type of low-lying excitations that potentially affects various properties in a crystal at low temperature.

In the β pyrochlores, specific heat experiments found low-energy contributions that could be described approximately by the Einstein model and determined the Einstein temperature T_E to be 70 K, 60 K, and 40 or 31 K for A = Cs, Rb, and K, respectively.[13, 14] This tendency illustrates uniqueness of the rattling, because, to the contrary, one expects a higher frequency for a lighter atom in the case of conventional phonons. Moreover, it was demonstrated that the specific heat shows an unusual T^5 dependence at low temperature below 7 K for A = Cs and Rb, instead of a usual T^3 dependence from a Debye-type phonon.[13] On one hand, structural refinements revealed large atomic displacement parameters at room temperature of $100U_{iso}$ = 2.48, 4.26, and 7.35 Å^2 for A = Cs, Rb, and K, respectively,[10] and 3.41 Å^2 for Rb.[15] Particularly, the value for K is enormous and may be the largest among rattlers so far known in related compounds. This trend over the β-pyrochlore series is ascribed to the fact that an available space for the A ion to move in a rather rigid cage increases with decreasing the ionic radius of the A ion.[10] Kuneš *et al*. calculated an energy potential for each A ion and found in fact a large anharmonicity, that is, a deviation from a quadratic form expected for the harmonic oscillator approximation.[16] Especially for the smallest K ion, they found 4 shallow potential minima locating away from the center (8*b* site) along the <111> directions pointing to the nearest K ions, as schematically shown in Fig. 1. The potential minima are so shallow that the K ion may not stop at one of them even at very low temperature.

The electronic structures of α-$Cd_2Re_2O_7$ and β-AOs_2O_6 have been calculated by first-principle density-functional methods, which reveal that a metallic conduction occurs in the (Re, Os)-O network:[16-20] electronic states near the Fermi level originate from transition metal 5*d* and O 2*p* orbitals. Although the overall shape of the density of states (DOS) is similar for the two pyrochlores, a difference in band filling may result in different properties; Re^{5+} for α-$Cd_2Re_2O_7$ has two 5*d* electrons, while $Os^{5.5+}$ for β-AOs_2O_6 has two and a half. Moreover, a related α-pyrochlore $Cd_2Os_2O_7$ with Os^{5+} ($5d^3$) exhibits a metal-to-insulator transition at 230 K.[21, 22]

Various experiments have been carried out on the pyrochlore oxide superconductors to elucidate the mechanism of the superconductivity. Most of the results obtained for α-$Cd_2Re_2O_7$ indicate that it is a weak-coupling BCS-type superconductor.[23, 24] In contrast, results on the β-pyrochlores are somewhat controversial. Although the T_c increases smoothly from Cs to K, the jump in specific heat at T_c, the upper critical field, and the Sommerfeld coefficient all exhibit a large enhancement toward K.[25] Thus, the K compound is always distinguished from the others. Pressure dependence of T_c was also studied for the two pyrochlores, showing a common feature: as pressure increases, T_c first increases, exhibits a broad maximum and goes to zero above a critical pressure that depends on the system, for example, about 6 GPa for the K compound.[26-29]

On the symmetry of the superconducting gap for the β-pyrochlores, Rb-NMR and μSR experiments gave evidence for *s*-wave superconductivity for $RbOs_2O_6$.[30-32] In contrast, Arai *et al*. carried out K-NMR experiments and found no coherence peak in the relaxation rate below T_c for KOs_2O_6, which seemed to indicate unconventional superconductivity.[32] However, their recent interpretation is that the absence of a coherence peak does not necessarily mean non-*s* pairing, because the relaxation rate probed by the K nuclei can be affected dominantly by strongly overdamped phonons.[33] Kasahara *et al*. measured thermal conductivity using a KOs_2O_6 single crystal and concluded a full

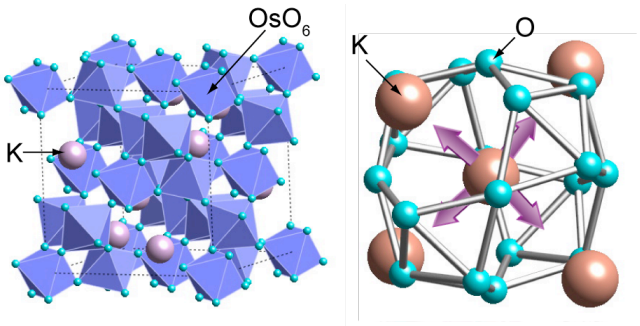

FIG. 1. (Color online) Crystal structure of the β-pyrochlore oxide KOs_2O_6. The K ion (big ball) is located in an oversized atomic cage made of OsO_6 octahedra and can move along the 4 <111> directions pointing to the neighboring K ions in adjacent cages.

gap from the insensitivity of thermal conductivity to magnetic fields.[34] Moreover, very recent photoemission spectroscopy (PES) experiments revealed the opening of a large isotropic gap below T_c.[35] On one hand, a μSR experiment claimed that the gap of KOs_2O_6 is anisotropic, or otherwise, there are two gaps.[36] Therefore, the pairing symmetry of the β-AOs_2O_6 superconductors may be of the conventional *s* wave, aside from minor aspects such as anisotropy or multi gaps, which means that the fundamental pairing mechanism is ascribed to phonons. Then, an important question is what kind of phonons are relevant for the occurrence. To find out the reason of the observed singular appearance toward K in the series must be the key to understand interesting physics involved in this system.

Previous studies have suffered poor quality of samples, because only polycrystalline samples were available. The Sommerfeld coefficient γ was estimated from specific heat by extracting contributions from Os metal impurity to be 40 mJ K^{-2} mol^{-1} for both Cs and Rb,[13] and 34 mJ K^{-2} mol^{-1} for Rb.[7] Recently, Brühwiler *et al*. obtained large values of γ = 76-110 mJ K^{-2} mol^{-1} for KOs_2O_6 by collecting five dozen of tiny crystals.[14] However, there is an ambiguity in their values, because of uncertainty in their extrapolation method. They also reported strong-coupling superconductivity with a coupling constant λ_{ep} = 1.0-1.6.[14] Recently, we successfully prepared a large single crystal of 1 mm size for KOs_2O_6 and reported two intriguing phenomena: one is a sharp and huge peak in specific heat at T_p = 7.5-7.6 K below T_c, indicative of a first-order structural transition,[37, 38] and the other is anisotropic flux pinning at low magnetic fields around 2 T.[39] It was suggested that the former is associated with the rattling freedom of the K ion. Moreover, anomalous concave-downward resistivity was observed down to T_c, suggesting a peculiar scattering mechanism of carriers.

In this paper, we present specific heat, magnetization and resistivity measurements on the same high-quality single crystal of KOs_2O_6. Reliable data on the superconducting and normal-state properties are obtained, which provide evidence for an extremely strong-coupling superconductivity realized in this compound. We discuss the role of rattling vibrations of the K ion on the mechanism of the superconductivity.

II. EXPERIMENTAL

A. Sample preparation

A high-quality single crystal was prepared and used for all the measurements in the present study, which was named KOs-729 after the date of July 29, 2005 when the first experiment was performed on this crystal. It was grown from a pellet containing an equimolar mixture of $KOsO_4$ and Os metal in a sealed quartz tube at 723 K for 24 h. Additional oxygen was supplied by using the thermal decomposition of AgO placed away from the pellet in the tube. The $KOsO_4$ powder had been prepared in advance from KO_2 and Os metal in the presence of excess oxygen. It was necessary to pay attention to avoid the formation of OsO_4 in the course of preparation, which is volatile even at room temperature and highly toxic to eyes or nose. After the reaction, several tiny crystals had grown on the surface of the pellet. Although the mechanism of the crystal growth has not yet been understood clearly, probably it occurs through partial melting and the following reaction with a vapor phase.

The KOs-729 crystal possesses a truncated octahedral shape with a large (111) facet as shown in Fig. 2 and is approximately 1.0 × 0.7 × 0.3 mm^3 in size and 1.302 mg in weight. The high quality of the crystal has been demonstrated by a sharp peak at T_p in specific heat,[38] which was absent in the previous polycrystalline samples or appeared as broad humps in our previous aggregate of tiny crystals[37] or in five dozen of tiny crystals by Brühwiler *et al*.[14] Moreover, a dramatic angle dependence of flux-flow resistance was observed on this crystal, indicating that flux pinning is enhanced in magnetic fields along certain crystallographic directions such as [110], [001], and [112].[39] This evidences the absence of domains in this relatively large crystal.

A special care has been taken to keep the crystal always in a dry atmosphere, because it readily undergoes hydration in air, as reported in isostructural compounds such as $KNbWO_6$.[40, 41] Once partial hydration takes place in KOs_2O_6, the second sharp anomaly in specific heat tends to collapse. In contrast, the superconducting transition was robust, just slightly broadened after hydration. The hydration must be relatively slow in a single crystal compared with the case of polycrystalline samples, which may be the reason for the broad anomaly or the absence in previous samples.

B. Physical-property measurements

Both specific heat and electrical resistivity were measured in a temperature range between 300 K and 0.4 K and in magnetic fields of up to 14 T in a Quantum Design Physical Property Measurement System (PPMS) equipped with a ^{3}He refrigerator. The magnetic fields had been calibrated by measuring the magnetization of a standard Pd specimen and also by measuring the voltage of a Hall device (F.W. BELL, BHA-921). Specific heat measurements

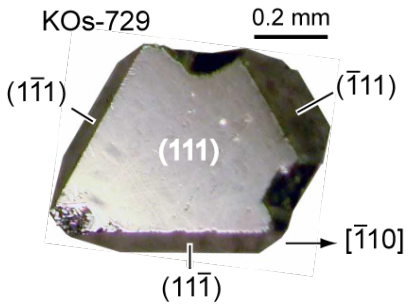

FIG. 2. (Color online) Photograph of the KOs-729 crystal used in the present study. It possesses a truncated octahedral shape with 111 facets. The approximate size is 1.0 × 0.7 × 0.3 mm^3. Resistivity measurements were carried out with a current flow along the [-110] direction.

were performed by the heat-relaxation method. The KOs-729 crystal was attached to an alumina platform by a small amount of Apiezon N grease. In each measurement, heat capacity was obtained by fitting a heat relaxation curve recorded after a heat pulse giving a temperature rise of approximately 2%. The heat capacity of an addendum had been measured in a separate run without a sample, and was subtracted from the data. The measurements were done three times at each temperature with a scatter less than 0.3% at most.

Resistivity measurements were carried out by the four-probe method with a current flow along the [-110] direction and magnetic fields along the [111], [110], [001] or [112] direction of the cubic crystal structure. All the measurements were done at a current density of 1.5 A cm^{-2}. Magnetization was measured in magnetic fields up to 7 T in a Quantum Design magnetic property measurement system and also up to 14 T in PPMS. The magnetic fields were applied approximately along the [111] or [-110] direction.

III. RESULTS

A. Superconducting properties

1. Specific heat

First of all, we analyze specific heat data in order to obtain a reliable value of the Sommerfeld coefficient γ. There are two obstacles: one is the large upper critical field H_{c2} that is approximately 2 times greater than our experimental limit of 14 T. Brühwiler *et al*. reported $\gamma = 76$ (110) mJ K^{-2} mol^{-1} assuming $\mu_0 H_{c2} = 24$ (35) T by an extrapolation method.[14] Their values should be modified to $\gamma \sim 100$ mJ K^{-2} mol^{-1}, because recent high magnetic field experiments revealed $\mu_0 H_{c2} = 30.6$ T or 33 T.[42, 43] Nevertheless, there are still large ambiguity in their extrapolation method using specific heat data obtained only at $H/H_{c2} < 0.5$. The other difficulty comes from unusual lattice contributions in specific heat at low temperature and the existence of a sharp peak at T_p. Thus, it is not easy to extract the lattice contribution in a standard way used so far. Here we carefully analyze specific heat data and reasonably divide them into electronic and lattice parts, from which a reliable value of γ is determined, and information on the superconducting gap is attained.

Figure 3 shows the temperature dependence of specific heat of the KOs-729 crystal measured on cooling at zero field and in a magnetic field of 14 T applied along the [111] direction. A superconducting transition at zero field takes place with a large jump, followed by a huge peak due to the second phase transition at $T_p = 7.5$ K. The entropy-conserving construction shown in the inset gives $T_c = 9.60$ K, $\Delta C/T_c = 201.2$ mJ K^{-2} mol^{-1}, which is close to the values previously reported,[14, 37] and a transition width (ΔT_c) of 0.3 K. T_c is reduced to 5.2 K at 14 T, which is evident as a bump in the 14-T data shown in Fig. 3. In contrast, Brühwiler *et al*. reported $T_c = 6.2$ K at 14 T, though the transition was not clearly observed in their specific heat data. The C/T at zero field rapidly decreases to zero as T approaches absolute zero. The absence of a residual T-linear contribution in specific heat indicates the high quality of the crystal.

The specific heat of a crystal (C) is the sum of an electronic contribution (C_e) and an H-independent lattice contribution (C_l). The former becomes C_{en} for the normal state above T_c, which is taken as γT, and C_{es} for the superconducting state below T_c. The γ is assumed to be T-independent, though it can not be the case for compounds with strong electron-phonon couplings.[44] In the case

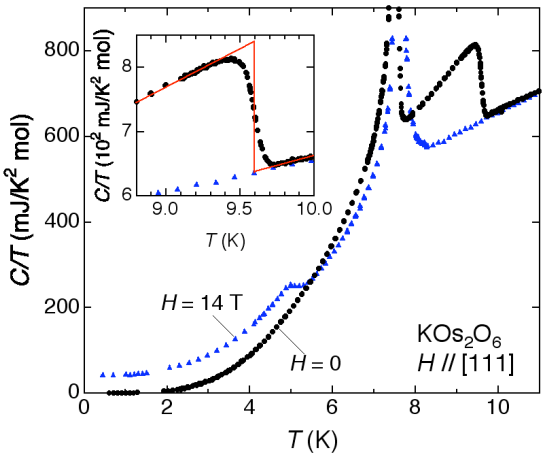

FIG. 3. (Color online) Specific heat divided by temperature measured at zero field (circle) and a magnetic field of 14 T (triangle) applied along the [111] direction. The inset shows an enlargement of the superconducting transition with an entropy-conserving construction.

of KOs_2O_6, C_l is large relative to C_e: for example, C_l is as large as ~90% of the total C at just above T_c, as shown later. In order to determine the value of γ, it is crucial to know the low-temperature form of C_l. Since the minimum T_c attained at 14 T is 5.2 K, one has to estimate the C_l from the T dependence of the total C above ~5.5 K. Two terms in the harmonic-lattice approximation are often required for an adequate fit; $C_l = \beta_3 T^3 + \beta_5 T^5$. The first term comes from a Debye-type acoustic phonon, and thus is dominant at low temperature, while the second term expresses a deviation at high temperature. Actually, this approximation is valid for α-$Cd_2Re_2O_7$, where $\beta_3 = 0.222$ mJ K^{-4} mol^{-1} and $\beta_5 = 2.70 \times 10^{-6}$ mJ K^{-6} mol^{-1} are obtained by a fit to the data below 10 K.[1] The Debye temperature Θ_D is 458 K from the β_3 value. In strong contrast, it was found for two members of β-AOs_2O_6 that the T^5 term prevails in a wide temperature range; $\beta_5 = 14.2 \times 10^{-3}$ mJ K^{-6} mol^{-1} below 5 K for $CsOs_2O_6$ and $\beta_5 = 30.2 \times 10^{-3}$ mJ K^{-6} mol^{-1} below 7 K for $RbOs_2O_6$.[13]

The C/T at $H = 0$ below 7 K shown in Fig. 3 is again plotted in two ways as functions of T^2 and T^4 in Fig. 4. It is apparent from the T^2 plot that possible T^3 terms expected for $\Theta_D = 458$ K and 300 K are negligibly small compared with the whole magnitude of specific heat, just as observed in other members. On the other hand, in the T^4 plot, there is distinct linear behavior at low temperature below 4 K, indicating that the C approaches asymptotically to T^5 behavior as $T \rightarrow 0$ with a large slope of 0.3481(6) mJ K^{-6} mol^{-1}. It is reasonable to ascribe this T^5 contribution to the lattice, because C_{es} should decrease quickly as $T \rightarrow 0$. Note that the value of the β_5 for KOs_2O_6 is more than one order larger than those in other members. At high temperatures above 4 K, a downward deviation from the initial T^5 behavior is observed in Fig. 4b. The temperature dependence of the 14-T data above 5.5 K, which is taken as $\gamma T + C_l$, is also close to T^5, but with a smaller slope, which means that a single T^5 term is not appropriate to describe the C_l in such a wide temperature range and also that an inclusion of higher order term of T^n is not helpful. Therefore, we adopt expediently an alternative empirical form to express this strange lattice contribution; $C_l = \beta_5 T^5 f(T)$, where $f(T) = [1 + \exp(1 - pT^{-q})]^{-1}$. Since the $f(T)$ is almost unity below a certain temperature and decreases gradually with increasing T, this C_l can reproduce T^5 behavior at low temperatures and a weaker T

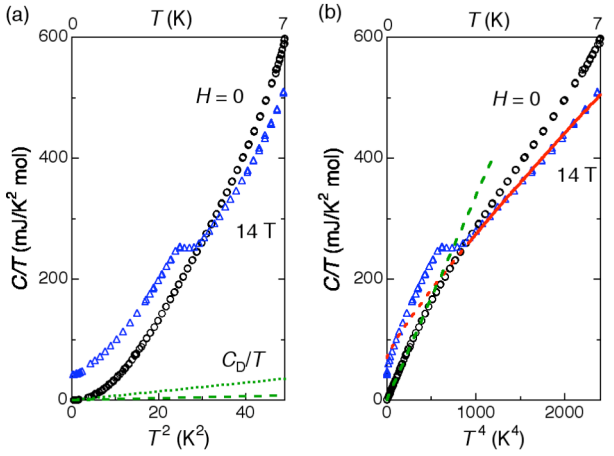

FIG. 4. (Color online) Low-temperature specific heat below 7 K plotted as functions of T^2 (a) and T^4 (b). The broken and dotted lines in (a) show calculated contributions from Debye T^3 phonons of Θ_D = 460 K and 300 K, respectively, which are much smaller than the experimental values. The broken line in (b) is a linear fit to the zero-field data as $T \rightarrow 0$, which gives a coefficient of the T^5 term, β_5 = 0.3481(6) mJ K^{-6} mol^{-1}. The solid and dotted line is a fit to $C_l = \beta_5 T^5 f(T)$. See text for detail.

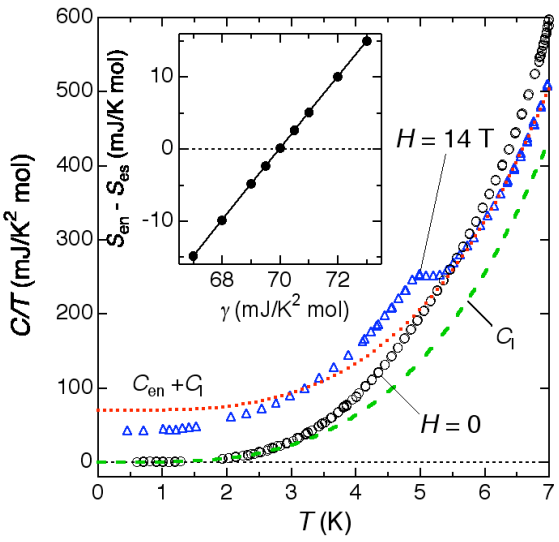

FIG. 5. (Color online) Specific heat data same as shown in Fig. 3. The dotted line shows the estimated contribution of $C_{en} + C_l$, and the broken line represents C_l in the case of γ = 70 mJ K^{-2} mol^{-1}. The inset shows a change of entropy balance as a function of γ, from which the value of γ is decided to be 70 mJ K^{-2} mol^{-1}.

dependence at high temperatures. As shown in Fig. 4b, the 14-T data in the 5.5-7 K range can be fitted well by the function for a value of β_5 fixed to the initial slope of 0.3481 mJ K^{-6} mol^{-1} and a given value of γ; for example, p = 6.96(3) and q = 1.09(1) for γ = 70 mJ K^{-2} mol^{-1}.

In order to determine the value of γ univocally, the entropy conservation is taken into account for the 14-T data, as shown in Fig. 5: since the normal-state specific heat expected for the case of T_c = 0 is given by ($C_{en} + C_l$) (dotted line in Fig. 5), the integration of $[C_{en} + C_l - C(14\ \mathrm{T})]/T$ should become zero due to entropy balance. It is shown in the inset to Fig. 5 that the integrated value changes almost linearly with γ and vanishes around γ = 70 mJ K^{-2} mol^{-1}. Hence, one can determine the value of γ unambiguously. A certain ambiguity may arise from the assumed lattice function. However, since the temperature dependence of C_l is substantially weak in the T range of interest, a possible correction on the γ value must be minimal, say, less than 1 mJ K^{-2} mol^{-1}.

Next we determine C_{es} at zero field by subtracting the C_l estimated above. The temperature dependence of C_{es} does have the BCS form, $a\exp(-\Delta/k_BT_c)$, as shown in Fig. 6. The energy gap Δ obtained by fitting is 22.5 K, which corresponds to $2\Delta/k_BT_c$ = 4.69, much larger than the BCS value of 3.53. The above C_{es} at low temperature below 7 K is again plotted in Fig. 7 together with high-temperature C_{es} above 5.5 K, which is obtained by subtracting the 14-T data from the zero field data as $C_{es} = C(0) - C(14\ \mathrm{T})$. The two data sets obtained independently overlap well in the 5.5-7 K range, assuring the validity of the above analyses. Because of the existence of the second peak and its small shifts under magnetic fields, the data between 7 K and 8.3 K is to be excluded in the following discussion. Taking γ = 70 mJ K^{-2} mol^{-1}, the jump in specific heat at T_c, $\Delta C/\gamma T_c$, reaches 2.87, much larger than 1.43 expected for a weak-coupling superconductor, indicating that KOs_2O_6 lies in the strong-coupling regime. Comparisons to other typical strong-coupling superconductors are made in section IV-B.

Here we analyze the data based on the α model that was developed to provide a semi-empirical approximation to the thermodynamic properties of strong-coupled superconductors in a wide range of coupling strengths with a single adjustable parameter, $\alpha = \Delta_0/k_BT_c$.[45] Recently, it was generalized to a multi-gap superconductor and successfully applied to the analyses on MgB_2 or Nb_3Sn.[46, 47] Using the α model, the data in the vicinity of T_c is well reproduced, as shown in Fig. 7, and we obtain α = 2.50 ($2\Delta_0/k_BT_c$ = 5.00), slightly larger than the value obtained above from the temperature dependence of C_{es}. One interesting point to be noted is that there is a significant deviation between the data and the fitting curve at intermediate temperatures, suggesting the existence of an additional structure in the gap. Presumably, this enhancement would be explained if one assumes the coexistence of another smaller gap (not so small as in MgB_2, but intermediate). This possibility has been already pointed out in the previous μSR experiment.[36] However, ambiguity associated with the second peak in the present data prevents us from further analyzing the data. This important issue will be revisited in future work, where the

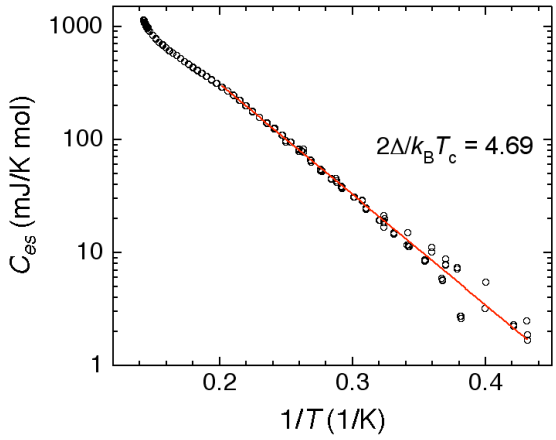

FIG. 6. (Color online) Temperature dependence of electronic specific heat measured at H = 0 for the superconducting state showing an exponential decrease at low temperature. A magnitude of the gap obtained is $2\Delta/k_BT_c$ = 4.69.

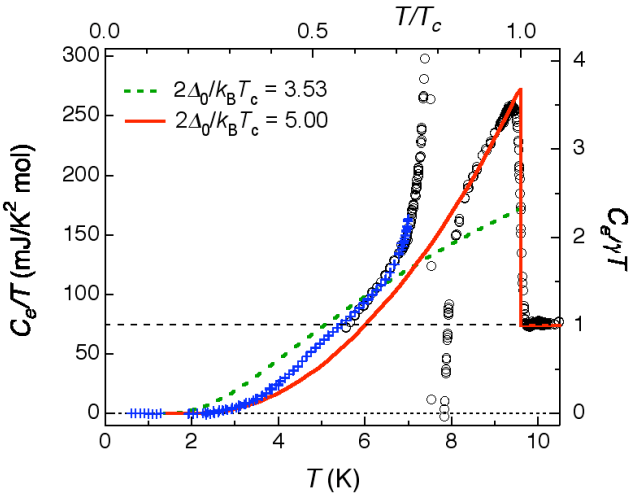

FIG. 7. (Color online) Electronic specific heat of KOs_2O_6 at zero field. The data points above 5.5 K (open circle) is obtained by subtracting the 14-T data from the zero-field data, and those below 7 K (cross) is obatined by subtracting the estimated lattice part C_l from the zero-field data. The broken line shows an ideal curve expected for a weak-coupling BCS superconductor, and the solid curve is a fit by the α model with a large value of gap; $2\Delta/k_BT_c$ = 5.00.

second peak in specific heat would be suppressed by hydration or a small amount of Rb substitution for K.

The thermodynamic critical field H_c is one of the most important parameters to characterize the nature of the superconducting ground state. It is determined from specific heat data taken at $H = 0$ using the relation,

$$\int_T^{T_c} dT \int_T^{T_c} \frac{C(T') - C_{en}(T')}{T'} dT' = \frac{H_c^2}{8\pi}. \qquad (1)$$

However, in the present case, H_c can be determined only in the vicinity of T_c due to the second anomaly in specific heat. Since H_c can be also determined by magnetization measurements, we will be back to this issue in the later section.

In the vortex state under magnetic fields, a finite amount of T-linear term $\gamma(H)T$ appears in specific heat well below T_c. Since the C/T is almost constant below 1 K, we take the value of C/T at 0.5 K as approximately giving $\gamma(H)$ at each field, and plots the magnetic field dependence in Fig. 8. It increases with a negative curvature and is approximately proportional to $H^{0.89}$. An extrapolation of the curve to $H = H_{c2}$ (30.6 T) would result in γ = 85.4 mJ K^{-2} mol^{-1}, which is larger than our estimate of γ = 70 mJ K^{-2} mol^{-1}. In a similar analysis, Brühwiler *et al.* found an $H^{0.95}$ curve with an extrapolated γ = 76 (110) mJ K^{-2} mol^{-1} for $\mu_0 H_{c2}$ = 24 (35) T.[14] The fact that γ = 70 mJ K^{-2} mol^{-1} in our experiments means that the magnetic field dependence is first expressed by a power of H and tends to saturate near H_{c2}. In general, $\gamma(H)$ is considered to probe the quasiparticle DOS in the vortex state: it is expected to increase linearly with H for a simple s-wave gap, while increase more rapidly for gaps with nodes. However, recent study on $YNi_2B_2C_2$ and $NbSe_2$ has demonstrated that a non-linear dependence actually appears even for an s-wave superconductor, when the system approaches the clean limit.[48] As will be mentioned later, the present superconductor lies in the very clean limit, and thus, the observed nonlinear behavior may be reconciled with an s-wave gap.

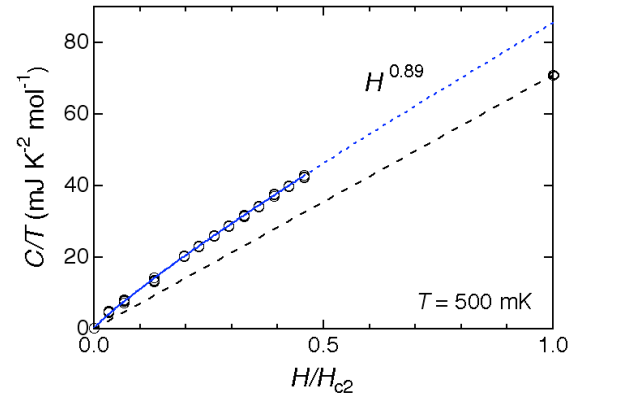

FIG. 8. (Color online) Magnetic-field dependence of C/T at T = 500 mK. The abscissa axis is normalized by the value of $\mu_0 H_{c2}$ = 30.6 T. The broken line assumes a linear H dependence with γ = 70 mJ K^{-2} mol^{-1} at $H/H_{c2} = 1$. The fit to the power law of H^n gives n = 0.89 and a large value of γ = 85.4 mJ K^{-2} mol^{-1} at $H/H_{c2} = 1$.

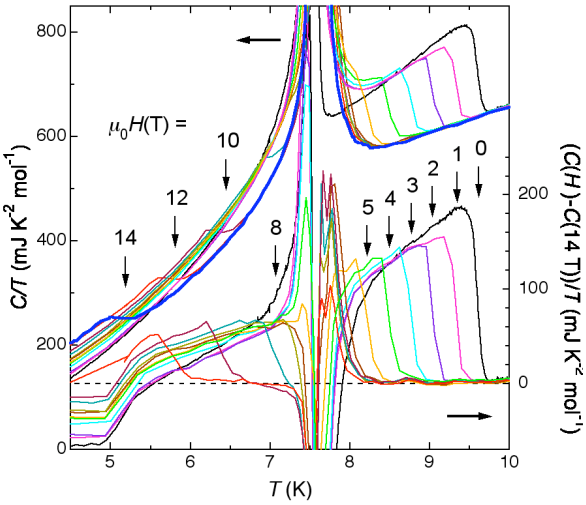

FIG. 9. (Color online) C/T measured at various magnetic fields on the left axis and the same data after subtraction of the 14-T data on the left. The magnetic fields are 0, 1, 2, 3, 4, 5, 6, 7, 8, 10, 12, and 14 T from right to left.

Let us describe next superconducting transitions in specific heat under various magnetic fields. As shown in Fig. 9, the jump at T_c systematically shifts to lower temperatures with increasing H, though the transition becomes obscure on the way in the vicinity of T_p. It is clearly observed that there are substantial differences between the transitions above and below T_p: in the case of $T_c > T_p$, the jump is large and sharp with a small ΔT_c, while it becomes small and broad for $T_c < T_p$. The H dependences of the mean-field T_c and $\Delta C/T_c$ are plotted in Figs.10 and 11, respectively. In the H-T diagram of Fig. 10, the superconducting phase is separated into two regions I and II by an almost vertical T_p line.[38] The H_{c2} increases first linearly, suddenly drops by 15% at T_p, and increases again linearly but with a smaller slope below T_p. The values of $-dH_{c2}/dT$ are 3.61(4) T/K and 3.20(5) T/K above and below T_p, respectively. The former value agrees with that reported by Brühwiler *et al.*, though they did not find a change in the slope across the T_p line.[14] A linear extrapolation of the low-temperature H_{c2} line intersects with the abscissa axis at T = 9.5 K, which is close to the T_c = 9.60 K. This naturally demands that the two

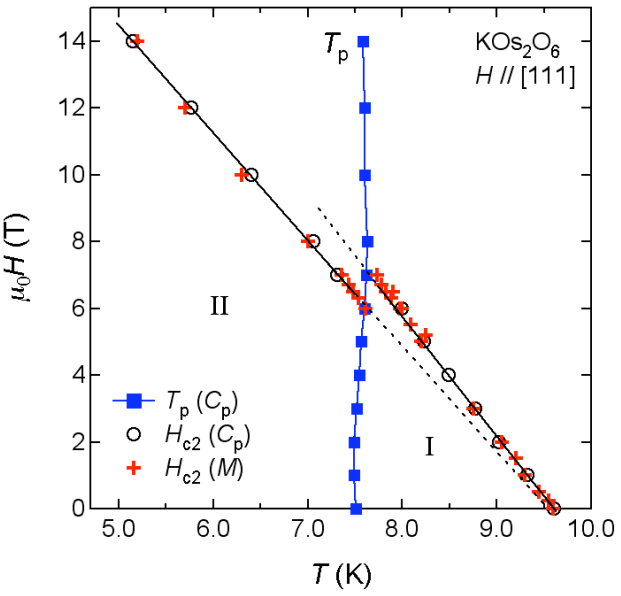

FIG. 10. (Color online) Magnetic field-temperature phase diagram obtained at H // [111] showing H_{c2} lines determined by specific heat (circle) and magnetization measurements (cross). The vertical line (square) indicates the position of the peak in specific heat associated with the second phase transition.

superconducting states are essentially identical in origin, but with slightly different parameters affected by the second phase transition. Details will be discussed later. On the other hand, a linear extrapolation of the two H_{c2} lines to $T = 0$ gives $\mu_0 H_{c2}(0) = 34.7$ T and 30.5 T, the latter of which agrees with the value obtained by high magnetic field experiments.[42] This fact suggests that the degradation of a sample that suppresses the second phase transition would enhance $H_{c2}(0)$. Certainly, a larger value of 33 T for $H_{c2}(0)$ was reported in another high magnetic field experiments.[43]

Another dramatic change at T_p is shown in Fig. 11 in the magnetic field dependence of the magnitude of the jump in specific heat. The $\Delta C/T_c$ decreases suddenly around a critical field of 6.5 T, where the H_{c2} and the T_p lines intersect. Liner extrapolations of

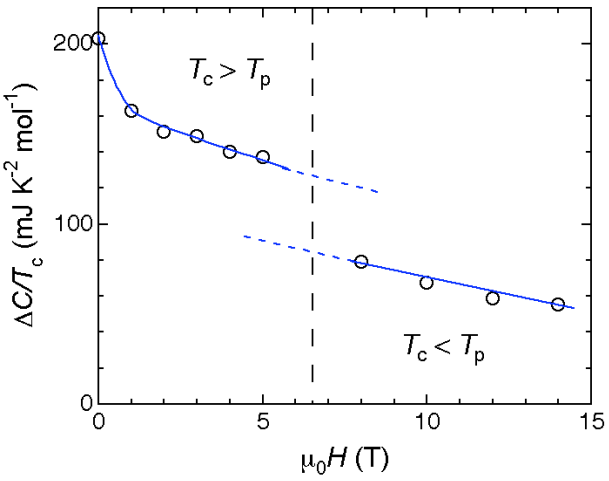

FIG. 11. (Color online) Magnetic field dependence of the magnitude of the jump in specific heat at T_c obtained from the data sets shown in Fig. 9. The vertical broken line shows a critical field at which T_c and T_p coincide with each other.

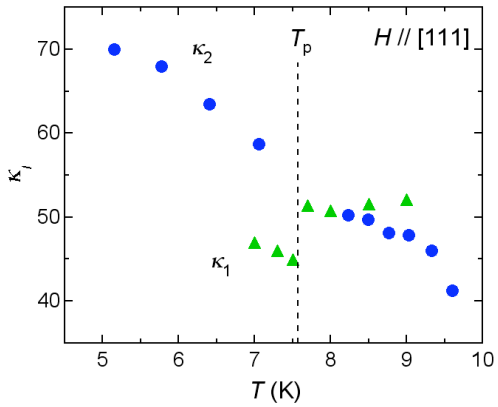

FIG. 12. (Color online) Temperature dependence of the Maki parameters, κ_1 and κ_2.

the curves above and below the critical field give a marginal discontinuity of approximately 42 mJ K^{-2} mol^{-1}, which means a reduction by 33% from the low-field value. $\Delta C/T_c$ is related to the slope of H_{c2} and the Maki parameter κ_2 as in the formula,

$$\left(\frac{\Delta C}{T_c}\right) = \frac{1}{4\pi\beta_A\left(2\kappa_2^2 - 1\right)}\left(\frac{dH_{c2}}{dT}\right)_{T_c}^2, \qquad (2)$$

where β_A =1.16 for a triangular vortex lattice.[49] Thus, the reduction of $\Delta C/T_c$ must be partly due to the reduction of $-dH_{c2}/dT$ observed in Fig. 10. However, since the change of $-dH_{c2}/dT$ is only ~15% (~2.3% in $(dH_{c2}/dT)^2$), it is required to assume a large enhancement of κ_2 at T_p. The T dependence of κ_2 is determined by Eq. (2) and is plotted in Fig. 12. The κ_2 increases with decreasing T from T_c, followed by an increment around T_p and shows a further increase at low temperature. The observed enhancement of κ_2 below T_p may indicate that the system goes more close the clean limit as a result of the second transition. Characteristic changes for various quantities observed at T_p are summarized and discussed in section IV-D. The T dependence of another Maki parameter κ_1 is also plotted in Fig. 12, which will be described later in section III-A-3.

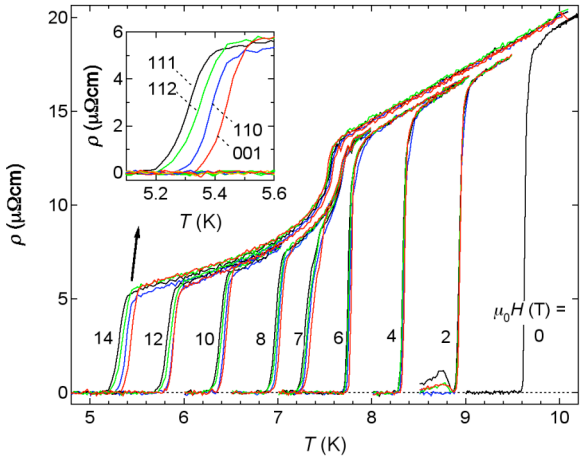

FIG. 13. (Color online) Temperature dependence of resistivity measured under various magnetic fields of up to 14 T in 4 crystallographic directions; [111], [112], [110], and [001]. The inset shows an enlargement near T_c for the 14-T data. Small humps observed just below T_c at 2 T are due to flux-flow resistance coming from weak and anisotropic pinning.[39]

2. Resistivity - anisotropy

The superconducting transition of the KOs-729 crystal observed by resistivity measurements has been already reported in our previous paper for magnetic fields parallel to the [111] direction.[38] Here we report further results for various field directions to reveal the anisotropy of the superconductivity. Figure 13 shows the temperature dependence of resistivity measured in magnetic fields along 4 principal directions of the cubic crystal; [111], [112], [110] and [001], which was obtained by rotating the crystal along the [-110] direction that was also the direction of current flow. It is apparent from Fig. 13 that there are only small anisotropy in the superconducting transition. The T_c becomes always higher in the sequence of H // [111], [112], [110] and [001], though the difference is small within 0.12 K even at the maximum field, as shown in the inset of Fig. 13. Therefore, KOs_2O_6 is an isotropic superconductor, reflecting the cubic symmetry of the crystal structure and also round Fermi surfaces predicted in the band structure calculations.[16, 19, 20, 25] Nevertheless, it is surprising that there is a distinct anisotropy in flux pinning as reported previously.[39] A sign is also shown in Fig. 13 in the sets of 2 T curves: there is a relatively large hump below a sharp drop for H // [111], intermediate ones for [112] and [001], and no hump for [110]. Such a hump was detected only around H = 1-2 T.

3. Magnetization

We have carried out magnetization measurements on the KOs-729 crystal. An advantage compared with specific heat is that magnetization is sensitive to the occurrence of superconductivity but may not be affected by the second phase transition in the normal state, as shown for the 7-T data in Fig. 14(a). This enables to probe a superconducting transition near T_p. First we describe the temperature dependence of magnetization measured in various magnetic fields on cooling. The T_c determined as an onset of diamagnetic signals due to the Meissner effect agrees with that from specific heat measurements at each field up to 14 T, as shown in the H-T diagram of Fig. 10. Figure 14(a) shows typical data in the vicinity of the second transition. For example, at $\mu_0 H$ = 5.5 T, a diamagnetic response starts at T_c(I) = 8.1 K and grows almost linearly on cooling, followed by an sudden upward departure at T = 7.75 K. Essentially the same temperature dependence was observed for data obtained below this field. Figure 14(b) shows the deviation of magnetization from the initial linear relation below T_c(I). It is apparent that the deviation always takes place at T_p' = 7.7 K at any magnetic fields. Hence, it is reasonable to correlate this H-independent anomaly in magnetization to the second peak in specific heat. Possibly, the superconducting volume fraction is partly suppressed at around T_p, associated with the reduction of H_{c2}. At higher magnetic fields above 6.0 T, another diamagnetic onset appears at a temperature below T_p, as shown in Fig. 14(a). For example, at $\mu_0 H$ = 6.0 T, there is a clear downturn at T_c(II) = 7.6 K. The two onset temperatures are plotted in the H-T diagram of Fig. 10, which exactly fall on the two H_{c2} lines above and below T_p determined by specific heat measurements, providing strong evidence for a discontinuity in H_{c2} at T_p. There must be an interesting vortex state between T_p and T_c(II) associated with the phase transition.

Next, we tried to determine the lower critical field H_{c1} from a magnetic field dependence of magnetization. Figure 15 shows a typical M-H curve measured at 2 K and H // [111] after zero-field

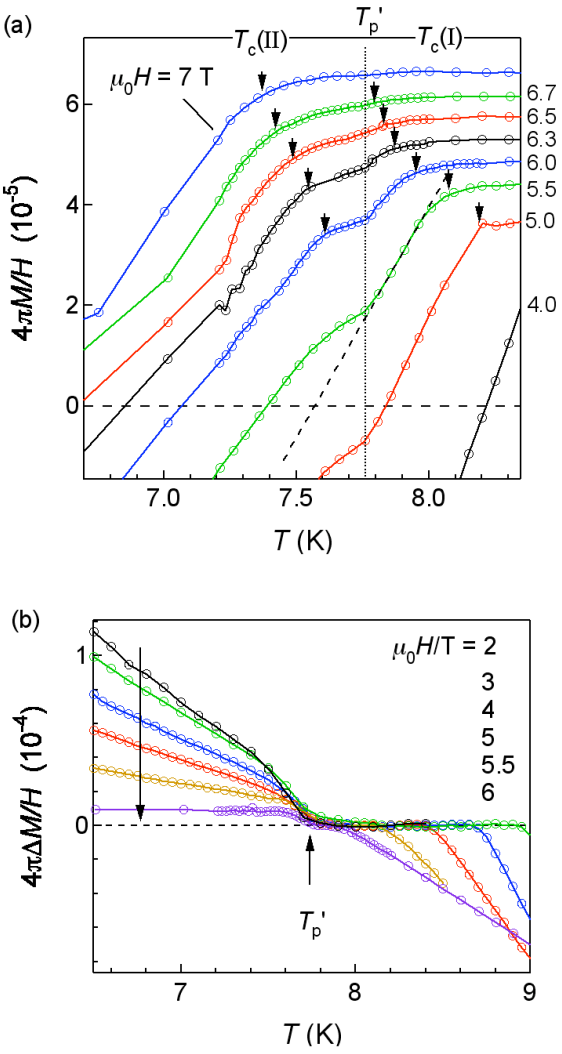

FIG. 14. (Color online) (a) Temperature dependence of magnetization measured on cooling at magnetic fields of up to 7.0 T in the [111] direction. Data sets at $\mu_0 H$ = 5.5, 6.0, 6.3, 6.5, 6.7, and 7.0 T are shifted upward relatively by an offset of 3 × 10^{-6} for clarity. (b) Deviation of the diamagnetic signal from the initial linear behavior such as shown in (a) for the 5.5-T data by a broken line. It always takes place at T_p' near T_p, independent of H.

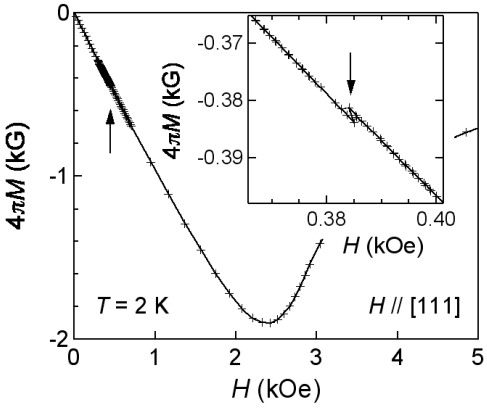

FIG. 15. (Color online) Virgin M-H curve measured at H // [111] and T = 2.0 K after zero-field cooling. The inset shows an enlargement around an anomaly marked by an arrow.

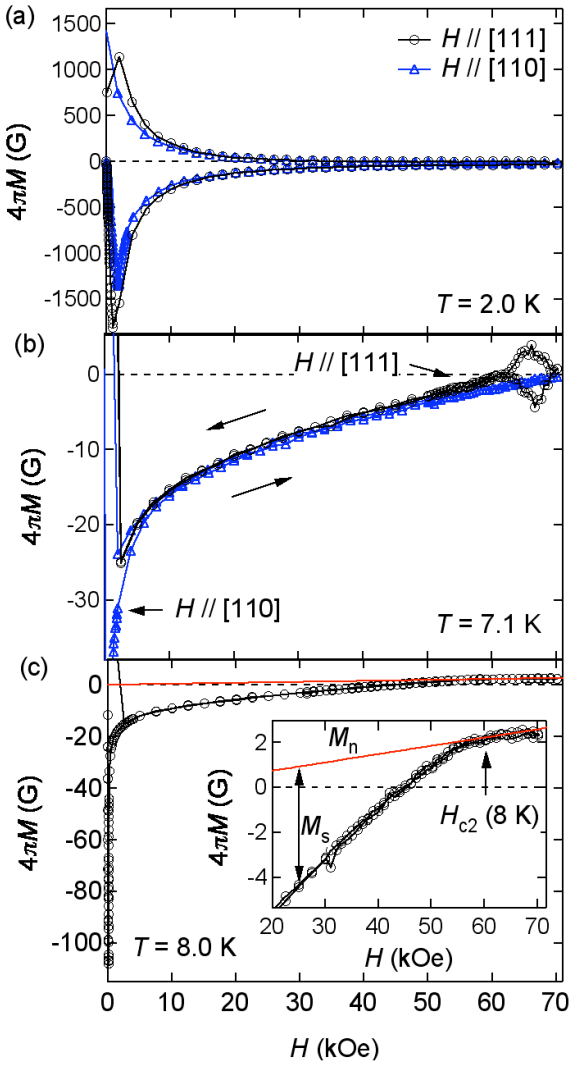

FIG. 16. (Color online) *M-H* curves measured at *H* // [111] (circle) and [110] (triangle) after zero-field cooling at $T = 2.0$ K (a), 7.1 K just below T_p (b), and 8.0 K above T_p (c). There is a hysteresis at 2.0 K, while an almost reversible change is observed at the two high temperatures. In (b), a peak effect is found near H_{c2} only at *H* // [111]. The inset shown in (c) is an enlargement near $\mu_0 H_{c2} = 6.0$ T at 8.0 K. M_s and M_n are magnetizations for the superconducting and normal states, respectively.

cooling. The correction due to the geometric demagnetization effect was determined from the initial slope assuming the perfect diamagnetism: the demagnetization factor was 0.586 and 0.269 for *H* // [111] and [110], respectively, larger for the former case as expected from the plate-like shape of the crystal, Fig. 2. H_{c1} is to be defined as a magnetic field where a deviation from the linear behavior starts. In fact, we observed a clear anomaly or a jump at $\mu_0 H = 35 \sim 40$ mT, as shown in the inset to Fig. 15. However, since the values scattered from experiment to experiment even in the same experimental setup, we could not determine a reliable value for H_{c1}. Possibly, this scattering is caused by a small misalignment of the crystal in a magnetic field. It is inferred from this that the effect of a surface barrier to flux inclusion is significantly large for this crystal. An expected value for H_{c1} from the Ginzburg-Landau (GL) relation is much smaller, ~10 mT, as described later.

Figure 16 shows the *H* dependence of magnetization measured at *H* // [111] and [110] and at $T = 2.0$ K, 7.1 K, and 8.0 K, after cooling in zero field. The shape of the *M-H* curves for $T = 2.0$ K shown in Fig. 16(a) is typical for a type II superconductor with a flux pinning. Since the area of the hysteresis loop is slightly larger for *H* // [111] than [110], the critical current density is larger for the former, though the anisotropy is small. At high temperatures just below T_p, *M-H* curves become almost reversible, as shown in Fig. 16(b), indicating a weak pinning. However, there is a small hysteresis loop appearing at high fields around 6.5 T only for *H* // [111], which means that a specific mechanism is working to enhance flux pinning. Such a peak effect has been discussed a lot in many superconductors and ascribed to various mechanisms. We think that in the present case a certain microstructure associated with the second phase transition at T_p is related to this peak effect. Details will be described elsewhere.

The Maki parameter κ_2 can be estimated in magnetization measurements near H_{c2} by the relation

$$\left(\frac{dM}{dH} - \frac{dM_n}{dH}\right)_{H_{c2}} = \frac{1}{4\pi\beta_A\left(2\kappa_2^2 - 1\right)}, \qquad (3)$$

where *M* is the magnetization of the vortex phase and M_n the magnetization of the normal phase.[49] As shown in Fig. 16(c) for $T = 8.0$ K, *M* increases with *H* and intersects an M_n line around 6.0 T, which is the H_{c2} determined by specific heat measurements. Since dM/dH near the H_{c2} is approximately 1.6×10^{-5}, and dM_n/dH is 2.9×10^{-6}, κ_2 is determined to be 50.8, which is in good agreement with that from specific heat measurements shown in Fig. 12. In other words, a thermodynamic relation[49]

$$\frac{1}{V_m}\left(\frac{\Delta C}{T}\right)_{T_H} = \left(\frac{dH_{c2}}{dT}\right)^2 \left(\frac{dM}{dH} - \frac{dM_n}{dH}\right)_{H_{c2}} \qquad (4)$$

holds, where V_m is the mol volume ($V_m = 77.277$ cm^3/mol), which confirms the reliability of our specific heat and magnetization data.

The thermodynamic critical field H_c is now determined in the vicinity of T_c, where hysteresis due to flux pinning is almost negligible, using the relation

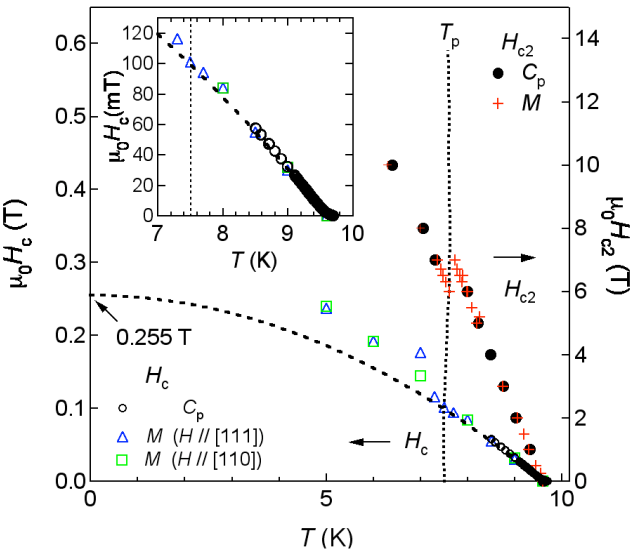

FIG. 17. (Color online) Thermodynamic critical field H_c determined by specific heat (open circle) and magnetization measurements at *H* // [111] (triangle) and *H* // [110] (square). The inset shows an enlargement near T_c and T_p. The broken line is a fit to the deviation function $D(t) = 0$, which gives $\mu_0 H_c(0) = 0.255$ T.

$$\int_0^{H_{c2}} (M - M_n)dH = \frac{H_c^2}{8\pi}, \qquad (5)$$

and is plotted in Fig. 17, together with the H_c determined by specific heat measurements using Eq. (1). The data from specific heat is limited above 8.5 K because of the existence of the second peak, while the data from magnetization below 7.0 K may be overestimated because of hysteresis due to flux pinning. As shown in the inset of Fig. 17, the two sets of data fall on the same line, showing a linear increase with an initial slope of -53.06 mT/K. This quantity is related to the jump in specific heat at T_c by a thermodynamic relation

$$\frac{1}{V_m}\frac{\Delta C}{T_c} = \frac{1}{4\pi}\left(\frac{dH_c}{dT}\right)^2_{T_c}. \qquad (6)$$

Using $\Delta C/T_c$ = 201.2 mJ K^{-2} mol^{-1} we obtain $-(dH_c/dT)_{Tc}$ = 57.2 mT/K, reasonably close to the above value. The temperature dependence of H_c is generally discussed in terms of a deviation function $D(t)$; $D(t) = H_c(t)/H_c(0) - (1-t^2)$, where $t = T/T_c$. It is known that $D(t)$ is always negative for a weak-coupling superconductor, while positive for a strong-coupling one.[49] In the present case, however, we can not obtain $D(t)$ in a wide T range, though $D(t)$ is expected to be positive for such a strong-coupling superconductor. Instead, we estimate $H_c(0)$ from the initial slope using a relation $H_c(0) = -(T_c/2)dH_c(T)/dT$ to be 0.255 T, which is to be used to deduce important parameters in the GL formulation.

It is also noted in Fig. 17 that the H_c is likely unaffected by the second phase transition. It seems that at least there is no reduction in H_c corresponding to the reduction in H_{c2} at T_p, which suggests no substantial differences in the condensation energy between the two superconducting states. From the values of H_{c2} and H_c, another Maki parameter κ_1 is calculated by $H_{c2} = \sqrt{2}\kappa_1 H_c$, and its temperature dependence is shown in Fig. 12. The κ_1 is almost constant, ~ 51, above T_p and coincides with κ_2 just above T_p, followed by a sudden reduction to 45 below T_p, corresponding to the change in H_{c2}. Thus, the ratio of κ_2/κ_1 is increased from ~1 at 8 K to 1.25 at 7 K. It is known for a conventional type-II superconductor such as Nb that the ratio of κ_2/κ_1 is sensitive to the purity of specimens and is enhanced for a specimen with a large mean free path.[50] Consequently, the enhanced κ_2/κ_1 ratio below T_p for KOs_2O_6 must imply that the electron mean free path is elongated below the second transition, which means that the system becomes cleaner below T_p.

B. Normal-state properties

1. Specific heat

Figure 18 compares the specific heat of the normal state in a wide temperature range for KOs_2O_6, $CsOs_2O_6$ and $Cd_2Re_2O_7$. It is obvious that, compared with $Cd_2Re_2O_7$, both the β-pyrochlores possess a large weight at low temperature, especially for KOs_2O_6, indicating the presence of low-energy phonons. Moreover, the specific heat at 300 K is considerably smaller than an ideal value of 27R per 1 mol of formula unit (fu) expected by Dulong-Petit's law. The reduction is greater toward KOs_2O_6. Since the Dulong-Petit limit should be attained for most solids in which the harmonic oscillator approximation for atomic vibrations is valid, this reduction means that the anharmonicity of the lattice is essentially large for pyrochlore oxides and more enhanced in the β-pyrochlores with larger rattlings.

In order to estimate the specific energy of rattling vibrations,

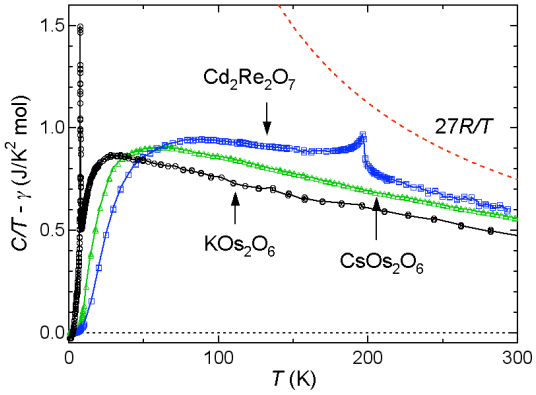

FIG. 18. (Color online) Specific heat in a wide temperature range below room temperature for KOs_2O_6 (KOs-729), $CsOs_2O_6$ (polycrystalline sample), and $Cd_2Re_2O_7$ (single crystal, reduced by 9/11 for comparison). The γ value has been subtracted. The broken line represents the Dulong-Petit limit.

we have fitted the data following by the method adopted for a similar analysis on filled skutterudites or Si/Ge clathrates.[11, 51] Although the anharmonicity must be crucial for rattling vibrations, it is difficult to take into account in the analysis. Thus, we assume that the rattler presents an Einstein oscillator, because it may be almost localized in a cage, and the Os-O framework gives a Debye phonon. Two terms are included for each contribution to reproduce the data, and thereby specific heat C per mol is given by

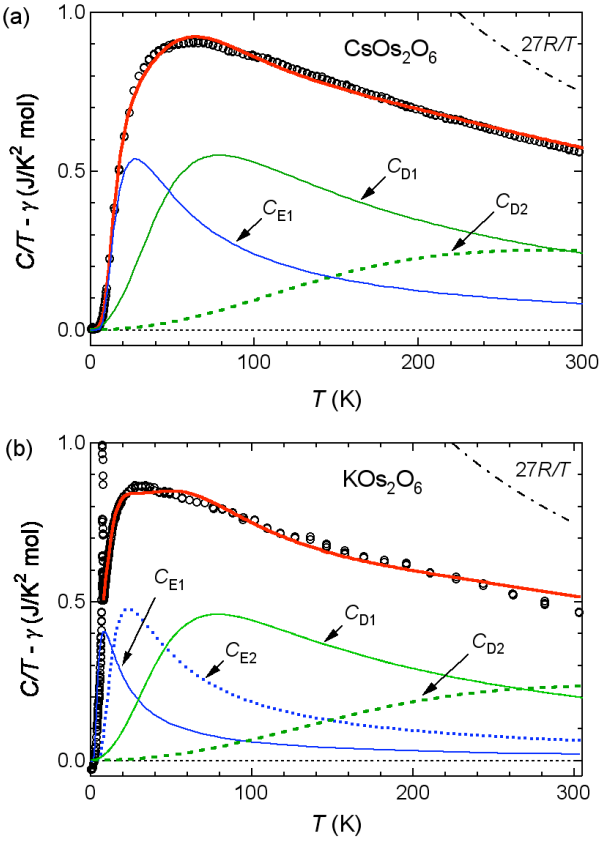

FIG. 19. (Color online) Results of fitting to the model described in the text for $CsOs_2O_6$ (a) and KOs_2O_6 (b). Separated contributions are shown below the raw data.

$$C = \gamma T + aC_{E1} + (1\text{-}a)C_{E2} + bC_{D1} + (8\text{-}b)C_{D2}, \quad (7)$$

where C_{D1} and C_{D2} are contributions from Debye phonons of the Os_2O_6 cage, and C_{E1} and C_{E2} are those from Einstein oscillators for the A cation, which take the form as

$$C_E = 3R\left(\frac{\Theta_E}{T}\right)^2 \frac{\exp(\Theta_E/T)}{[\exp(\Theta_E/T)-1]^2}, \quad (8)$$

where R is the gas constant, and Θ_E is the Einstein temperature. The results of fitting are satisfactory, as shown in Fig. 19. In the case of $CsOs_2O_6$, the second Einstein contribution was not required to fit the data in the whole temperature range, and we obtained that $b = 3.05(3)$, $\Theta_{E1} = 70.5(2)$ K, $\Theta_{D1} = 280(2)$ K, and $\Theta_{D2} = 1000(6)$ K. The last term of such a large Debye temperature may be unrealistic, but is necessary to allow for the reduction from the Dulong-Petit limit at high temperatures. In contrast, we can not fit the data of KOs_2O_6 above 8.5 K without the second Einstein term. Although the results of fitting is improved by including the second term, there remains still a significant deviation for K, compared with the case for Cs. This implies that anharmonicity is greater in K. We finally obtain for K that $a = 0.24(3)$, $b = 2.55(4)$, $\Theta_{E1} = 22(2)$ K, $\Theta_{E2} = 61(1)$ K, $\Theta_{D1} = 280(3)$ K, and $\Theta_{D2} = 1180(13)$ K. The value of $\Theta_{E1} = 22$ K is smaller than the previous estimations giving 40 K[13] and 31 K[14], which assumed a single Einstein term. Although this harmonic approximation is not enough to describe the rattling, the obtained lowest value of Θ_{E1} may give a rough estimate for the characteristic energy of the rattling.

The fact that the rattling frequency is lower for K than Cs reveals one interesting aspect of rattling. In the ordinary solid, an atom with a smaller mass M gives a higher frequency ω, as ω is proportional to $M^{1/2}$. For the rattling, in contrast, frequency must be determined by the shape of energy potential in an oversized cage, just as in an electron confined in a quantum well. Indeed, Kunes *et al*. found such a quantum-well like potential for the K cation and calculated the energy diagram, where a triplet state exists above a singlet ground state separated by a small energy difference of 15 K.[16] According to their energy diagram, we calculated the specific heat, but could not reproduce the experimental curve. Further experimental and theoretical studies would be necessary to elucidate the nature of the rattling phenomena.

The origin of the T^5 behavior observed at low temperature is another mystery. In general, specific heat is proportional to $T^{3/n}$ for an excitation wave in three dimension with a dispersion relation of $\hbar\omega = q^n$ in the low temperature limit. For example, a Debye phonon with $\hbar\omega = q$ gives the T^3 law, while spin waves in ferromagnetic materials with $\hbar\omega = q^2$ gives C proportional to $T^{3/2}$. In this context, the present T^5 behavior means a strange excitation with $\hbar\omega = q^{3/5}$, though such an excitation wave with a power smaller than unity seems unrealistic. The fact that the coefficient β_5 of the T^5 term increases from Cs to K and is enhanced much for K suggests that the origin is also related to the rattling. We should bear in mind that the T^5 behavior is not directly related to the presence of the second transition present only for KOs_2O_6.

2. Resistivity

Since the rattler has a bare 1+ charge that must be screened effectively by the surrounding conduction electrons in the cage, one expects significantly large scattering of carriers due to an electron-phonon or electron-rattler coupling. This is possibly related to the anomalous temperature dependence of electrical resistivity commonly observed for the β-pyrochlore oxides. The resistivity of $CsOs_2O_6$ and $RbOs_2O_6$ exhibits a concave-downward

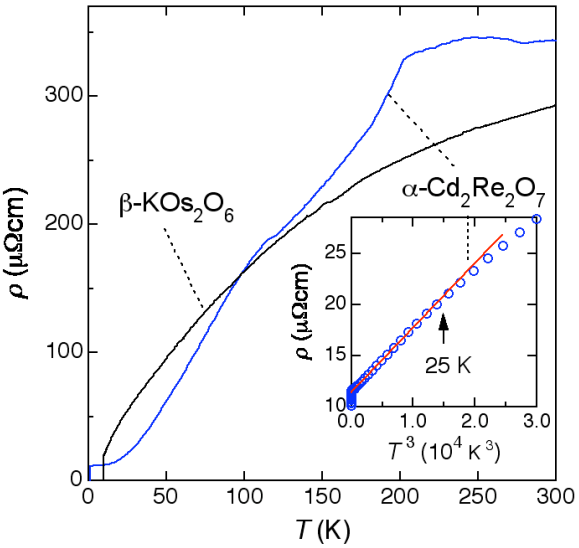

FIG. 20. (Color online) Resistivity in a wide temperature range for β-KOs_2O_6 and α-$Cd_2Re_2O_7$. The former exhibits always a concave-downward curvature down to T_c, while the latter shows a T^3 dependence at low temperature below 25 K, as represented in the T^3 plot of the inset. Two anomalies at 200 K and 120 K for the latter are due to structural transitions.[52]

curvature at high temperature, followed by T^2 behavior at low temperature below $T^* \sim 20$ K and ~ 15 K, respectively.[25] In contrast, such a crossover to a T^2 dependence is absent in KOs_2O_6, always concave-downward down to T_c, as shown in Fig. 20. On the other hand, α-$Cd_2Re_2O_7$ exhibits quite different behavior in resistivity that is proportional to T^3 below 25 K after two reductions at 120 K and 200 K due to structural transitions, as also shown in Fig. 20.[52] The origin of this T^3 behavior has not yet been understood, but is probably ascribed to an electron-phonon scattering due to certain low-energy phonons. The effect of electron correlations may be minor in α-$Cd_2Re_2O_7$.

As already shown in Fig. 13, the normal-state resistivity drops

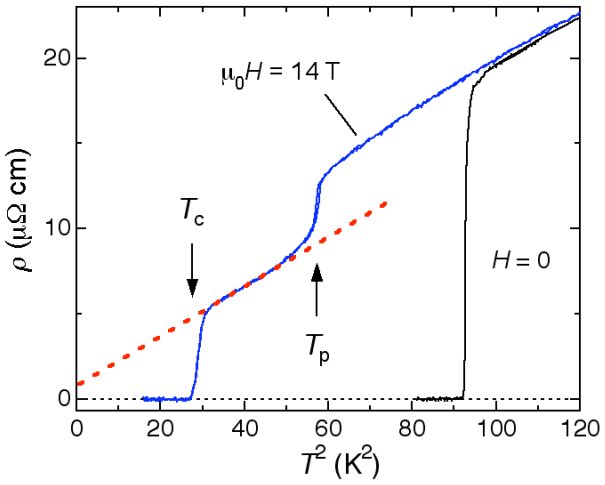

FIG. 21. (Color online) Resistivity plotted against T^2 near T_c for KOs_2O_6. A large reduction is observed at T_p in the 14-T data, where a small thermal hysteresis is deteced between the cooling and heating curves. A change from concave-downward to T^2 behavior across T_p is observed at the 14-T data. An extrapolation to $T = 0$ gives a residual resistivity $\rho_0 = 1$ μΩ cm.

suddenly at T_p in high magnetic fields. Figure 21 reproduces the 14-T data plotted as a function of T^2, where the T_c is reduced to 5.2 K. The magnitude of the drop observed at T_p is approximately 30%, which corresponds to an enhancement in conductivity by 27%. Moreover, the temperature dependence below T_p is apparently proportional to T^2, as shown in Fig. 21. These changes of the normal-state resistivity must imply that the scattering mechanism of carriers is substantially changed at T_p. Consequently, commonly observed in the resistivity of the β pyrochlores is the change from high-temperature concave-downward to low-temperature T^2 behavior, which takes place as a crossover at T^* for Cs and Rb, while as a phase transition at T_p for K. The former temperature dependence suggests a strong electron-phonon interaction possibly ascribed to the rattling of the *A* cations, while the latter may indicate that electron-electron scattering dominates at low temperature, as suggested also by recent thermal conductivity measurements.[34] However, there is no corresponding enhancement in χ, as will be describe later. We think, alternatively, that certain electron-phonon scatterings give rise to the T^2 resistivity, as in the case of another strong-coupling superconductors with the A-15 structure.[53]

A T^2 extrapolation to $T = 0$ gives a small residual resistivity, $\rho_0 \sim 1$ μΩ cm. Since the room temperature resistivity is ~300 μΩ cm, the residual resistivity ratio (RRR) reaches 300, which is unusually large for transition metal oxides. For example, the RRR of a $Cd_2Re_2O_7$ crystal shown in Fig. 20 is only 30. The residual resistivity is generally given as

$$\rho_0 = \frac{\hbar\left(3\pi^2\right)^{1/3}}{e^2 \ell n^{2/3}}, \qquad (9)$$

where l and n are the mean free path and the density of carriers, respectively. Although the latter has not yet been determined experimentally, band structure calculations gave $n = 2.8 \times 10^{21}$ cm^{-3} (18% per Os).[25] Assuming this value, we obtain a large l of 640 nm, which is comparable to the value of the most cleanest crystal of Sr_2RuO_4.[54] Since the superconducting coherence length ξ is 3.3 nm, much smaller than l, KOs_2O_6 lies definitely in the regime of the clean limit.

Next we will extract more information from the anomalously *T*-dependent resistivity. It is known that a class of intermetallic compounds having the A-15 structure such as Nb_3Sn show a similar temperature dependence of resistivity.[55] It shows T^2 or T^3 behavior above T_c up to ~50 K and then a concave-downward increase to be saturated at around $\rho = 100 \sim 150$ μΩ cm.[56] This saturation has been interpreted to be the Ioffe-Regel limit:[57] the electron mean free path becomes of the order of the interatomic spacing of the compound. It was pointed out that such an extremely short phonon-limited mean free path occurs when the Fermi velocity v_F is small and the electron-phonon coupling constant λ_{ep} is large (v_F/λ_{ep} is small).[58] That is really the case for the A-15 compounds; $v_F \sim 2 \times 10^7$ cm/sec and $\lambda_{ep} \sim 1.5$.

Wiesmann *et al.* analyzed the resistivity of A-15 compounds and introduced a phenomenological formula,[59]

$$\frac{1}{\rho} = \frac{1}{\rho_{\text{ideal}}} + \frac{1}{\rho_{\max}}, \qquad (10)$$

where the saturation resistivity $\rho_{\max}$ is presumed to be independent of temperature. At high temperature, the "ideal" resistivity can be written as $\rho_{\text{ideal}} = \rho_0 + \rho_1 T$ with T linear behavior as expected by the Bloch-Grüneisen theory. They obtained by fitting experimental data for Nb_3Sn $\rho_0 = 57$ μΩ cm, $\rho_1 = 0.532$ μΩ cm/K, and $\rho_{\max} = 130$ μΩ cm, which corresponds to a phonon-limited mean free path $l_{ep} \sim 5$ Å.

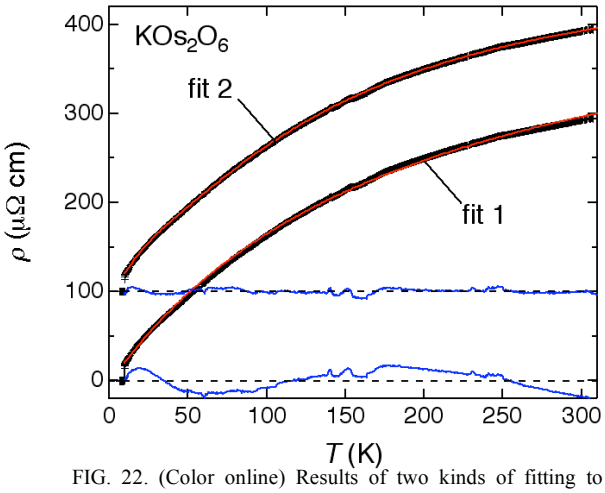

FIG. 22. (Color online) Results of two kinds of fitting to the resistivity data shown in Fig. 20. In each case, a solid line on the data points shows a fit, and a curve near $\rho = 0$ (100) μΩ cm in fit 1(2) shows a deviation that is expanded by a factor of five.

We apply Eq. (10) to the resistivity of KOs_2O_6. The results of fitting is fairly good, as shown in Fig. 22 (fit 1), yielding $\rho_0 =$ -4.9(3) μΩ cm, $\rho_1 = 2.535(7)$ μΩ cm/K, and $\rho_{\max} = 487(5)$ μΩ cm. The Ioffe-Regel limit ρ_{IR} is given as $\rho_{IR} = 3\hbar a/e^2$, where a is the interatomic distance. The ρ_{IR} of the pyrochlore oxides becomes 430 μΩ cm with $a = 3.6$ Å, which is nearly equal to the above experimental value of $\rho_{\max}$. Therefore, the observed saturation of resistivity in KOs_2O_6 is well understood as indicating an extremely short mean free path limited by electron-phonon scatterings. In fact, for KOs_2O_6, v_F is small, ~ 1.5×10^7 cm/sec,[20] and λ_{ep} is large, 2.4, as deduced later, which makes the ratio of v_F/λ_{ep} a factor of 2 smaller than in A-15 compounds.

Although the above fit 1 is satisfactory and reasonable at high temperature, it shows a slight deviation in the intermediate temperature range. An alternative analysis carried out by Woodard and Cody on the resistivity of A-15 compounds was to assume a selective electron phonon scattering.[55] They found an empirical formula

$$\rho = \rho_0 + \rho_1 T + \rho_2 \exp\left(-T_0/T\right) \qquad (11)$$

and could reproduce well the experimental curve for Nb_3Sn with $\rho_0 = 10$ μΩ cm, $\rho_1 = 0.0466$ μΩ cm/K, $\rho_2 = 74.7$ μΩ cm, and $T_0 = 85$ K. The characteristic energy $k_B T_0$ was interpreted as the energy of relevant phonons effective for scattering. In this analogy, we fit our data for KOs_2O_6 by assuming 2 exponential terms,

$$\rho_2 \exp\left(-T_{R1}/T\right) + \rho'_2 \exp\left(-T_{R2}/T\right), \qquad (12)$$

with characteristic temperatures of T_{R1} and T_{R2}, as shown in Fig. 22, fit 2. The results are almost perfect, giving $\rho_0 = 12.6(3)$ μΩ cm, $\rho_1 =$ -0.081(4) μΩ cm/K, $\rho_2 = 131(1)$ μΩ cm, $T_{R1} = 27.6(3)$ K, $\rho_2' =$ 326(2) μΩ cm, and $T_{R2} = 171(1)$ K. The T_{R1} is much smaller than T_0 for Nb_3Sn and close to the Einstein temperature $T_{E1} = 22$ K from specific heat. It follows from this that the low-energy phonons detected in specific heat is probably responsible for the strong electron-phonon scattering resulting in the observed anomalous concave-downward temperature dependence of resistivity for KOs_2O_6.

3. Magnetic susceptibility

We have measured the normal-state magnetic susceptibility χ of the KOs-729 crystal. Previously, we measured χ using a

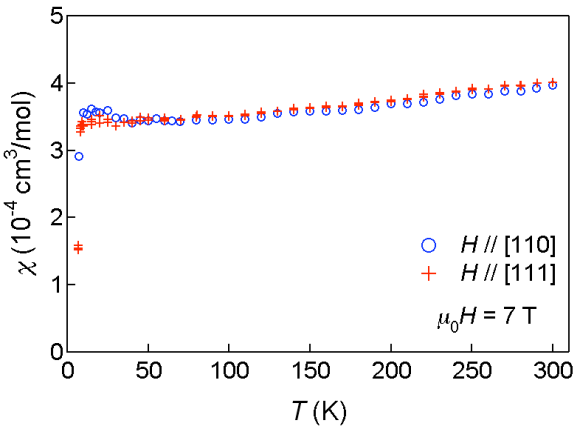

FIG. 23. (Color online) Magnetic susceptibility of the normal state measured at 7 T and H // [111] and [110].

polycrystalline sample and found a large temperature dependence. However, it turned out to be due to a small amount of an impurity phase that was a magnetic insulator. Here we carefully carried out χ measurements using the KOs-729 crystal and could obtain a reliable data.

Figure 23 shows χ measured in a magnetic field of 7 T applied along the two crystallographic directions, [111] and [110]. The anisotropy is negligibly small. They show essentially a T-independent Pauli paramagnetism with no signature of Curie-Weiss behavior at high temperature such as observed in a related α-pyrochlore oxide $Cd_2Os_2O_7$.[22] Therefore, electron correlations are not so large in KOs_2O_6. Nevertheless, it exhibits a weak temperature dependence with a positive slope, the origin of which is not known. We take the value of χ as $\chi = 3.4 \times 10^{-4}$ cm^3/mol at $T = 10$ K. This value is small compared with those for metallic 3d transition metal oxides and is slightly smaller than that of $Cd_2Re_2O_7$, $\chi = 4.8 \times 10^{-4}$ cm^3/mol.

In general, the magnetic susceptibility of metallic compounds is given as the sum of three terms: $\chi = \chi_s + \chi_{dia} + \chi_{orb}$, where they come from electron spins, core diamagnetism, and orbitals, respectively. We would like to know the first spin term from the experimental value. χ_{dia} is determined from literatures to be -1.2×10^{-4} cm^3/mol for KOs_2O_6. The orbital term must be significantly large for such a 5d transition metal oxide with a large spin-orbit interaction. In fact, in the case of $Cd_2Re_2O_7$, χ_{orb} was determined to be 3.16×10^{-4} cm^3/mol from the K-χ plot using the temperature dependence of Knight shift K from Cd NMR measurements.[60] Thus, $\chi_s = 3.16 \times 10^{-4}$ cm^3/mol was obtained for $Cd_2Re_2O_7$ ($\chi_{dia} = -1.52 \times 10^{-4}$ cm^3/mol). In the case of KOs_2O_6, the value of χ_{orb} has not yet been determined. If one assumes the same value as for $Cd_2Re_2O_7$, $\chi_s = 1.4 \times 10^{-4}$ cm^3/mol would be obtained, while $\chi_s = 4.6 \times 10^{-4}$ cm^3/mol when χ_{orb} is ignored. Pauli paramagnetic susceptibility χ_P expected from band structure calculations is $\chi_P = 2\mu_B^2 N(0) = 1.58 \times 10^{-4}$ cm^3/mol, which is close to the former value. It seems that the Stoner enhancement may not be so large in the present compound.

IV. DISCUSSION

A. Critical fields and fundamental superconducting parameters

In this section, we collect the values of the main thermodynamic and superconducting parameters obtained experimentally, which are listed in Table I, and discuss them and their relations to each other in the framework of the GL theory. In the extreme type-II limit 3 critical magnetic fields H_{c2}, H_c, and H_{c1} are related to each other by only 2 characteristic length scales, superconducting coherence length ξ and magnetic penetration depth λ, and their ratio $\kappa = \lambda/\xi$ by the equations[49]

$$H_{c2} = \frac{\phi_0}{2\pi\xi^2}, \tag{13}$$

$$H_c = \frac{\phi_0}{2\pi\sqrt{2}\lambda\xi}, \tag{14}$$

$$H_{c1} = \frac{\phi_0}{4\pi\lambda^2}\left[\ln\left(\frac{\lambda}{\xi}\right) + 0.08\right], \tag{15}$$

where ϕ_0 is the quantum flux.

Table I . Superconducting and normal-state parameters for α-pyrochlore $Cd_2Re_2O_7$ and β-pyrochlore KOs_2O_6.

	α-$Cd_2Re_2O_7$	β-KOs_2O_6
T_c (K)	1.0	9.6
$\mu_0 H_{c2}$ (0) (T)	0.29	30.6[a]
$\mu_0 H_c$ (0) (mT)	15	255
$\mu_0 H_{c1}$ (0) (mT)	2	9.4
ξ (nm)	34	3.3
λ (nm)	460	270[b]
GL parameter	14	84
$\Delta C/\gamma T_c$	1.15	2.87
$2\Delta(0)/k_B T_c$	3.5	5.0
γ_{exp} (mJ K^{-2} mol^{-1})	30.2	70
γ_{band} (mJ K^{-2} mol^{-1})	11.5	9.6-11.4
χ_s (10^{-4} cm^3 mol^{-1})	3.16	1.4[c]
χ_{band} (10^{-4} cm^3 mol^{-1})	1.8	1.5-1.8

[a]From high-magnetic field experiments by Ohmichi *et al.*[42]
[b]From μSR measurements by Koda *et al.*[36]
[c]Approximate value obtained by subtracting $\chi_{orb} = 3.16 \times 10^{-4}$ cm^3/mol.

Although the H_{c2} of KOs_2O_6 is much larger than our experimental limit of 14 T, two high-magnetic field experiments have already been reported. Ohmichi measured a magnetic penetration by the RF impedance method using a tunnel diode oscillator on a single crystal in high magnetic fields of up to 40 T and obtained $\mu_0 H_{c2}(0) = 30.6$ T.[42] On the other hand, Shibauchi *et al.* carried out similar measurements as well as resistivity measurements up to 50 T and determined $\mu_0 H_{c2}(0) = 33$ T.[43] It seems that there are some scatters in the value of H_{c2}, possibly resulting from the quality of crystals or the effects of the second phase transition. In fact, H_{c2} is lowered in a sample with a clear sign of the second transition, as shown in Fig. 10. It is well known that H_{c2} depends on the magnitude of the mean free path; a cleaner sample shows a lower H_{c2}.[49] Thus, we take the lowest value of $\mu_0 H_{c2}(0) = 30.6$ T in the following discussion, which gives $\xi = 3.3$ nm. Note that this may be the value for the low-temperature phase II, and that of the high-temperature phase I can be slightly smaller because of the larger H_{c2}.

We have obtained $\mu_0 H_c(0) = 0.255$ T from the initial slope of $H_c(T)$ determined by specific heat and magnetization measurements.

Thus, λ is calculated to be 278 nm from Eq. (14), which is in good agreement with $\lambda = 270$ nm from μSR measurements.[36] It follows from these values that the GL parameter κ is $\kappa = \lambda/\xi = 84$, certainly indicating that KOs_2O_6 is a type-II superconductor.

H_{c1} is estimated from Eq. (15) to be 9.4 mT, which is much smaller than found in our magnetization measurements. However, as already mentioned, this discrepancy may be due to an extrinsic effect.

The large value of H_{c2} for KOs_2O_6 was first considered as a sign of exotic superconductivity, because it was much larger than a Pauli limiting field $\mu_0 H_P = 18.6$ T expected from $\mu_0\mu_B H_{c2} = \Delta(0)/\sqrt{2}$ for $\Delta(0) = 1.76 k_B T_c$.[8] However, the actual value of H_P should be greater than this due to the larger gap, the strong coupling correction by a factor of $(1+\lambda_{ep})^{1/2}$, and the effect of spin-orbit scattering. Taking $2\Delta(0) = 4.57\ k_B T_c$ and $\lambda_{ep} = 1.6$ led Brühwiler *et al*. to obtain $\mu_0 H_P = 37$ T.[14] Alternatively, we obtain $\mu_0 H_P = 47$ T based on our estimations of $2\Delta(0) = 5.00\ k_B T_c$ and $\lambda_{ep} = 2.4$. It is known that spin-orbit scattering can also enhance H_{c2} in a dirty superconductor by reducing the effects of spin paramagnetism.[49] However, this effect may not be crucial in the present compound in the clean limit. Therefore, the experimental value of H_{c2} should be considerably smaller than H_P, and may be understood within the spin singlet scenario.

On the other hand, Shibauchi *et al*. estimated the value of H_P in a different way.[43] H_P is defined as a field where the condensation energy of Cooper pairs becomes comparable with the Zeeman energy of electron spins. Using equation

$$H_c^2/8\pi = \chi_n H_P^2/2, \qquad (16)$$

where χ_n is the susceptibility in the normal state, and $\chi_n = 4.2 \times 10^{-4}$ cm^3/mol and $\mu_0 H_c = 0.26$ T, they obtained $\mu_0 H_P = 31$ T. We obtain a similar value from the corresponding values of $\chi_n = 4.6 \times 10^{-4}$ cm^3/mol and $\mu_0 H_c = 0.255$ T in the present work. However, in order to estimate a true value of H_P in this way, one has to take spin susceptibility χ_s instead of χ_n. Although there is some ambiguity in the value of χ_s, as mentioned before, χ_s may be smaller than χ_n, as in the case of α-$Cd_2Re_2O_7$. Thus, H_P is expected to be larger than 31 T. For example, taking $\chi_s = 1.4 \times 10^{-4}$ cm^3/mol yields $H_P = 53$ T, which is close to the above estimation from the large gap and the strong-coupling correction. In any case, the actual value of H_{c2} is significantly smaller than H_P. Shibauchi *et al.* also pointed out that the temperature dependence of H_{c2} is somewhat strange, exhibiting an almost linear increase without saturations as $T \rightarrow 0$, and suggested an exotic mechanism for the enhancement based on the missing spatial inversion symmetry.[43]

B. Strong-coupling superconductivity

Present specific heat measurements as well as previous μSR, PES, and thermal conductivity measurements all gave strong evidence for an *s*-wave superconductivity occurring in KOs_2O_6. In addition, there are no evidence to show the existence of exotic excitations such as magnetic or charge fluctuations that can mediate the Cooper pairing. Thus, it is most likely to assume a phonon-mediated superconductivity for KOs_2O_6.

Three important quantities to characterize an isotropic superconducting ground state are $\Delta C(T_c)/\gamma T_c$, $\Delta(0)/k_B T_c$ and $\gamma T_c^2/H_c(0)^2$. Obtained in the present study are $\Delta C(T_c)/\gamma T_c = 2.87$, $\Delta(0)/k_B T_c = 5.00$ and 4.69 from the analysis of specific heat data by the α model and the temperature dependence of C_{es}, respectively, and $\gamma T_c^2/H_c(0)^2 = 0.128$. These values are compared in Fig. 24 and Table II with those for typical strong-coupling superconductors

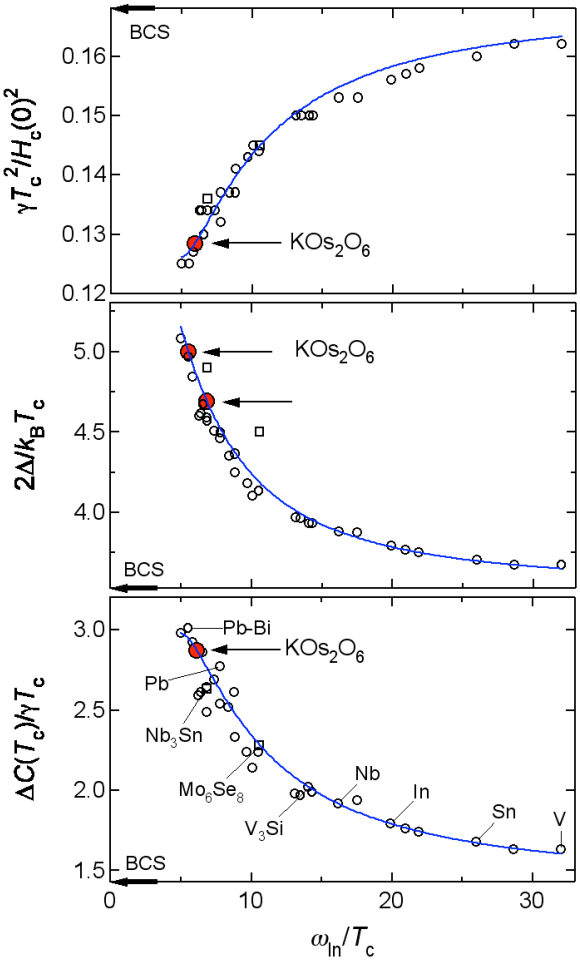

FIG. 24. (Color online) Three important quantities characterizing the strong-coupling superconductivity as a function of the average phonon frequency ω_{ln} normalized by T_c. Each mark represents a superconductor: open circle corresponds to those studied by Carbotte,[44] and squares to some Chevrel phase compounds.[60] The data of KOs_2O_6 is represented by a large solid circle. There are two data points in the middle panel: the upper one is obtained from the analysis of specific heat data using the α model (Fig. 7) and the lower from the low-temperature fit shown in Fig. 6. A curve on each plot shows an analytical form given in the text which represents a strong-coupling correction to a BCS ratio.

such as Pb and its alloys, A-15 and Chevrel phase compounds.[44, 61] Among all the known phonon-mediated superconductors, KOs_2O_6 possesses almost the largest values for $\Delta C(T_c)/\gamma T_c$ and $\Delta(0)/k_B T_c$, while the smallest value for $\gamma T_c^2/H_c(0)^2$, except for some Pb-Bi alloys, indicating that it is to be classified as an extremely strong-coupling superconductor. Then, a crucial question is what kind of phonons are relevant for such an extremely strong-coupling superconductivity. Particularly, the role of low energy phonons suggested by specific heat and resistivity measurements is to be considered.

We investigate the characteristic phonon frequency ω_{ln} and the electron-phonon coupling strength following the previous analyses developed for superconductors in the strong-coupling regime.[44] The corrections of the BCS values by strong electron-phonon interactions have been deduced in the following approximate analytic formulas that link a single parameter $x = \omega_{ln}/T_c$ to experimental thermodynamic quantities:

$$\frac{\Delta C(T_c)}{\gamma T_c} = 1.43\left[1 + \frac{53}{x^2}\ln\left(\frac{x}{3}\right)\right], \quad (17)$$

$$\frac{2\Delta(0)}{k_B T_c} = 3.53\left[1 + \frac{12.5}{x^2}\ln\left(\frac{x}{2}\right)\right], \quad (18)$$

$$\frac{\gamma T_c^{\,2}}{H_c(0)^2} = 0.168\left[1 - \frac{12.2}{x^2}\ln\left(\frac{x}{3}\right)\right]. \quad (19)$$

$\omega_{\ln}$ is the average phonon frequency given by

$$\omega_{\ln} = \exp\left[2\int_0^\infty d\omega\alpha^2 F(\omega)\ln\omega/\lambda_{ep}\omega\right], \quad (20)$$

where α^2 is the average electron-phonon interaction, $F(\omega)$ is the phonon DOS, and λ_{ep} the electron-phonon coupling constant. The three quantities for various superconductors are plotted as a function of $\omega_{\ln}/T_c$ together with the corresponding analytical curve in Fig. 24.

For KOs_2O_6, using Eq. (17) and $\Delta C(T_c)/\gamma T_c$ = 2.87, one obtains x = 6.14 or $\omega_{\ln}$ = 58.9 K. Using Eq. (18) and the gap values $\Delta(0)/k_BT_c$ = 5.00 and 4.69 from the analysis of specific heat data by the α model and the temperature dependence of C_{es}, respectively, one arrives at $\omega_{\ln}$ = 53.0 K and 65.7 K. Eq. (19) and $\gamma T_c^2/H_c(0)^2$ = 0.128 give $\omega_{\ln}$ = 57.2 K. Thus obtained three values of $\omega_{\ln}$ are in good agreement with each other, which confirms the validity of applying the above strong-coupling corrections to KOs_2O_6. On one hand, if one takes the value of $\Delta C(T_c)/\gamma T_c$ = 2.87 as the most reliable experimental data, the values of $\Delta(0)$ and $H_c(0)$ are determined alternatively by Eqs. (18) and (19) with $\omega_{\ln}$ = 58.9 K; $\Delta(0)/k_BT_c$ = 4.84 and $\gamma T_c^2/H_c(0)^2$ = 0.129 ($\mu_0 H_c(0)$ = 0.254 T).

Next, an electron-phonon coupling constant λ_{ep} can be estimated from the McMillan-Allen-Dynes equation with $\omega_{\ln}$ = 58.9 K;[62]

$$T_c = \frac{\omega_{\ln}}{1.2}\exp\left[\frac{-1.04(1+\lambda_{ep})}{\lambda_{ep} - \mu^*(1+0.62\lambda_{ep})}\right], \quad (21)$$

where μ^* is the Coulomb coupling constant and has been estimated to be 0.091 for KOs_2O_6.[20] We obtain λ_{ep} = 2.38, which is much larger than λ_{ep} = 1.6 reported previously.[14] It is also surprisingly large compared with those for typical strong-coupling superconductors like Pb (λ_{ep} = 1.55, $\omega_{\ln}$ = 50 K), Mo_6Se_8 (λ_{ep} = 1.27, $\omega_{\ln}$ = 70 K) and a Bi-Pb alloy (λ_{ep} = 1.7-2.1, $\omega_{\ln}$ = 50-45 K), as compared in Fig. 25 and Table II. An exceptionally large value of λ_{ep} = 2.59 was reported for an amorphous $Pb_{0.45}Bi_{0.55}$ thin film that was prepared by rapid quenching beyond the solubility limit.[62] It is interesting to note in Fig. 25 that the data point of KOs_2O_6 seems to lie slightly apart from a universal curve for other

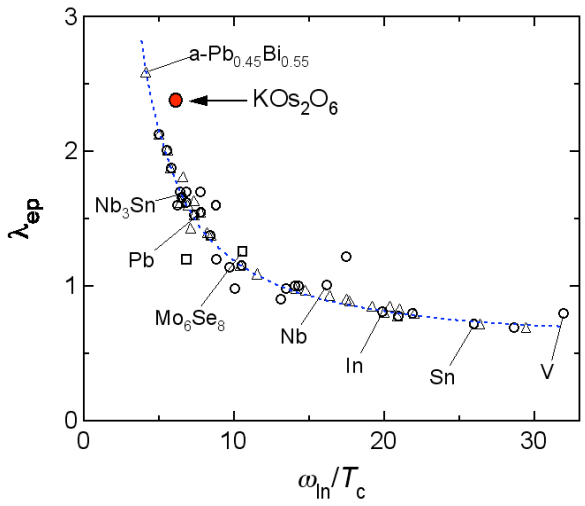

FIG. 25. (Color online) Electron-phonon coupling constant λ_{ep} versus $\omega_{\ln}/T_c$. Triangles are from Allen and Dynes,[61] and the other marks are the same as in Fig. 24. The broken line is a guide to the eye. KOs_2O_6 possesses the second largest λ_{ep}, next to an amorphous $Pb_{0.45}Bi_{0.55}$ film.

compounds, suggesting the uniqueness of the electron-phonon coupling in this compound. In the case of $\lambda_{ep} > 2$, however, there is a question about the validity of Eq. (21) to apply. Thus, assuming $\omega_{\ln}$ = 58.9 on the universal curve in Fig. 25, one obtains λ_{ep} = 1.8 alternatively. Anyway, since the λ_{ep} is relatively large, this assures us that there is a very strong electron-phonon coupling in KOs_2O_6.

The origin of the large λ_{ep} can not be attributed to usual phonons. Saniz and Freeman calculated the value using Θ_D = 285 K in a standard phonon-mediated pairing scenario and obtained a much smaller value of λ_{ep} = 0.85.[20] Since the λ_{ep} is expressed by

$$\lambda_{ep} = 2\int d\omega\alpha^2 F(\omega)/\omega, \quad (22)$$

a low-energy phonon may enhance λ_{ep} effectively: the low-energy part of $\alpha^2F(\omega)$ becomes dominant due to the denominator ω. In fact, many strong-coupling superconductors with large values of λ_{ep} possess various low-energy phonons. For example, the A-15 compounds show soft phonon modes associated with a cubic-to-tetragonal transition,[63] while the Chevrel phase compounds are assumed to be "molecular crystals" with low-lying phonon modes.[64] The role of such low-energy phonons on the mechanism of superconductivity has been studied extensively in these strong-coupling superconductors.

It is reasonable for KOs_2O_6 to ascribe such a low-energy phonon to the rattling vibration. The relevant phonon frequency $\omega_{\ln}$ = 58.9 K obtained from the above strong-coupling corrections

Table II. Comparison of superconducting parameters for typical strong-coupling superconductors.

	KOs_2O_6	$Cu_{1.8}Mo_6S_8$	Mo_6Se_8	Nb_3Sn	Nb	Pb	$Pb_{0.8}Bi_{0.2}$	a-$Pb_{0.45}Bi_{0.55}$	BCS
T_c (K)	9.6	10.8	6.34	18.1	9.25	7.20	7.95	7.0	
λ_{ep}	2.38	1.20	1.26	1.67	0.85	1.55	1.88	2.59	
$\omega_{\ln}$ (K)	58.9	74	67	125	166	56	46	29	
γ (mJ K^{-2} mol^{-1})	70	36.9	47.2	52.4	7.79	2.98	2.92		
$\Delta C/\gamma T_c$	2.87	2.63	2.28	2.5	1.87	2.71	1.43		1.43
$2\Delta(0)/k_BT_c$	5.00	4.9	4.5	4.7	3.66	3.95	4.843		3.53
$\gamma T_c^2/H_c^2$	0.128	0.136	0.145	0.134	0.155	0.132	0.127		0.168

should give an exponential average over the whole phonon DOS. The lower bound has been estimated to be T_{E1} = 22 K from specific heat and T_{R1} = 27.6 K from resistivity, which must enhance λ_{ep} effectively. Moreover, one expects large electron-phonon couplings for KOs_2O_6 because of the low Fermi velocity, as discussed for the saturated behavior of resistivity: slower electrons feel more the motion of surrounding ions, especially when the ions also move slowly with low energy.

It should be emphasized that in most cases the lattice itself becomes unstable when the electron-phonon coupling becomes too strong. In the present compound, however, conduction electrons are located on the hard skeleton made of OsO_6 octahedra, while low-energy phonons are associated with the rattling K ions that are weakly, structurally coupled to the skeleton, Fig. 1. This structural duality must give rise to such an unusually large coupling constant over 2. It would be intriguing to investigate further in detail how this rattling, which is an essentially anharmonic vibration almost localized in a cage, can mediate the Cooper pairing in KOs_2O_6. More experimental information, particularly from neutron diffraction experiments that can determine the low-energy phonon DOS, is required for further discussion.

C. Electronic structure and mass enhancement

According to electronic band structure calculations, 5*d* pyrochlore oxides possess commonly a strongly hybridized band made of transition metal 5*d* and O 2*p* states near the Fermi level, which is a manifold of 12 bands with a total bandwidth of ~3 eV. Because of the large bandwidth, they may not be classified as strongly correlated electron systems in the ordinary sense. However, since the profile of the DOS exhibits many sharp peaks due to a large degeneracy coming from the high symmetry of the pyrochlore structure, the magnitude of electron correlations may depend on the band filling. A calculated DOS at the Fermi Level is $N(0)$ = 2.45 states/eV fu (γ_{band} = 11.6 mJ K^{-2} mol^{-1}) for KOs_2O_6 with $Os^{5.5+}$ ($5d^{2.5}$),[20] which is larger than $N(0)$ = 1.14 states/eV fu (γ_{band} = 5.4 mJ K^{-2} mol^{-1}) for $Cd_2Re_2O_7$ with Re^{5+} ($5d^2$)[17] and smaller than $N(0)$ = 6.35 states/eV fu (γ_{band} = 29.9 mJ K^{-2} mol^{-1}) for $Cd_2Os_2O_7$ with Os^{5+} ($5d^3$). [22] Thus, one may expect a moderately large electron correlations for KOs_2O_6.

The calculated Fermi surface of β-AOs_2O_6 consists of a pair of closed sheets around the zone center and a hole-like sheet near the zone boundary.[16, 19, 20, 25] The former Fermi surface possesses a characteristic shape: each sheet is not spherical but close to an octahedron with flat surfaces, suggesting an electronic instability due to Fermi surface nesting.[19] However, there has been no experimental evidence to show the nesting instability. It would be interesting, if these two Fermi surfaces are related to the two superconducting gaps suggested in the specific heat data shown in Fig. 7.

The Sommerfeld coefficient calculated from the values of $N(0)$ given by the band structure calculations is approximately 10 mJ K^{-2} mol^{-1}, which is a factor of 7 smaller than the present experimental value. On the other hand, Pauli paramagnetic susceptibility calculated by $\chi_P = 2\mu_B^2 N(0)$ is 1.58 × 10^{-4} cm^3/mol, which may be similar or not so small compared with the experimental value. As a result, the Wilson ratio R_W, which is given by

$$R_W = \left(\pi^2/3\right)\left(k_B/\mu_0\right)^2\left(\chi_s/\gamma\right) = 72.949\left(\chi_s/\gamma\right), \qquad (24)$$

is estimated to be 0.15 (0.48) from γ = 0.070 J K^{-2} mol^{-1} and χ_s = 1.4 (4.6) × 10^{-4} cm^3/mol, smaller than unity. This small R_W means that only γ is enhanced. Therefore, the source of the mass enhancement should not be usual electron correlations, but probably electron-phonon interactions. The renormalization factor $(1 + \lambda_{ep})$ due to electron phonon interactions becomes 3.4 for λ_{ep} = 2.4 from the above estimation, which is still a factor of 2 smaller than the observed mass enhancement. Brühwiler *et al*. assumed a mass enhancement by a factor of $(1 + \lambda_{ep})(1 + \lambda_c)$ with an additional enhancement by $(1 + \lambda_c)$ that is ascribed to electron correlations. This may give a reasonable explanation, because we observed in fact a T^2 dependence for low-temperature resistivity. The coefficient A of the T^2 term is 0.143 μΩ cm K^{-2} and the γ value of 70 mJ K^{-2} mol^{-1} yield the Kadowaki-Woods ratio of A/γ^2 = 2.8 × 10^{-5}, close to the universal value of 10^{-5} for the strongly correlated electron system. Recent thermal conductivity experiments also pointed out the importance of electron correlations in KOs_2O_6.[34] Then, we obtain λ_c = 1.1. Nevertheless, it should be kept in mind that there is already a factor of 3 enhancement in γ for $Cd_2Re_2O_7$ that lacks electron correlations (no T^2 dependence in resistivity) as well as low-energy phonons such as observed in KOs_2O_6.

A large mass enhancement that is possibly associated with rattling vibrations has been found in the filled skutterudite $SmOs_4Sb_{12}$.[65] Miyake *et al*. studied an impurity four-level Kondo model, in which an atom is tunneling among 4 stable sites and interacting with surrounding conduction electrons, and found that the interaction can result in a moderate enhancement of the quasiparticle mass.[66] It is likely that the same mechanism is responsible for the mass enhancement for KOs_2O_6, because a similar situation is realized in KOs_2O_6, where 4 shallow potential minima for the K ion exist in a cage that allow a large excursion for the K ion from the center of the cage, as schematically illustrated in Fig. 1. It is likely that some entropy associated with the rattling survives at low temperature and gives rise to a heavy quasiparticle mass through a strong electron-rattler interaction. It would be necessary to test theoretically how large enhancement is in fact attainable through this exotic mechanism.

D. Effects of the second phase transition

Finally, we discuss on what happens for the superconducting and normal-state properties at the second phase transition that is presumably of structural origin. Thermal hysteresis observed in resistivity and specific heat implies that it is of first order. In our recent structural analysis, neither symmetry change nor cell doubling was detected. However, we found that the intensity of some reflections changed slightly at the transition. Details of the structural refinements will be described elsewhere.[67] It is remarkable that such a structural transition occurs below a superconducting transition, because in most cases an inherent lattice instability has been already lifted by coupling with electrons to induce superconductivity. It is also surprising that the superconductivity is certainly affected, but the influence is very small. Although the origin of the transition is so interesting, we leave the door to this issue open for future study.

Here we describe the observed effects of the transition on various properties. There must be little change in the band structure, especially, in the DOS at the transition, because the normal-state susceptibility is scarcely affected by the transition, as shown for the 7-T data in Fig. 14(a). Moreover, the fact that the specific heat at 14 T shown in Fig. 3 seems to be smoothly connected across the peak at T_p means no large change in the γ value. Consequently, the observed reduction in the normal-state resistivity at T_p must be ascribed to the enhancement of the mean free path or the lifetime of carriers: the associated increase of the mean free path is estimated

to be $\Delta l \sim 27\%$. In addition, the observed change in the temperature dependence from concave-downward to T^2 behavior means that an incoherent electron-rattler scattering has disappeared below T_p, resulting in this large enhancement of mean free path. Recent thermal conductivity experiments indicated in fact that the lifetime of carriers is largely enhanced below T_p.[34]

For the superconducting properties, on the other hand, the H_{c2} is decreased by 15% at T_p, and the ratio of the Maki parameters κ_2/κ_1 is increased by approximately 25%. In contrast, the fundamental superconducting parameters are preserved across the transition: both the T_c and H_c may be identical. Therefore, the observed changes in H_{c2} and the Maki parameters imply just that the system becomes closer to the clean limit and are compatible with the enhancement of the mean free path. Since H_{c2} is expressed as

$$H_{c2} = \frac{\phi_0}{2\pi\xi^2} \approx \frac{\phi_0}{2\pi\xi_0 \ell} \approx 3\times10^4 \frac{T_c}{v_F \ell}, \qquad (25)$$

where ξ_0 is the BCS coherence length,[68] ΔH_{c2} = -15% means that the l is enhanced by 17% at T_p. Therefore, all the observed changes at the second phase transition are at least qualitatively understood by assuming an enhancement in the mean free path, suggesting that a strong incoherent electron-rattler scattering has gone at the transition. This suggests that there is a substantial difference in the dynamics of rattlers across the transition.

IV. CONCLUSION

We have studied the superconducting and normal-state properties of the β-pyrochlore oxide KOs_2O_6 by means of specific heat, magnetization, and resistivity measurements. Various superconducting parameters are successfully determined, all of which give evidence for an extremely strong-coupling *s*-wave superconductivity. It is demonstrated that low-energy phonons having an average frequency of 58.9 K are responsible for the paring mechanism. Moreover, a very large electron-phonon coupling constant λ_{ep} of 2.38 is deduced from the strong-coupling corrections for the BCS values. The existence of the corresponding low-lying phonons is found in specific heat as well as resistivity that exhibits a concave-downward temperature dependence due to a large electron-phonon interaction.

The source of the low-lying phonons is ascribed to the rattling vibration of the K ion. Since the K ion is located in a highly anharmonic potential generated by the surrounding oversized metallic cage, it can rattle even at low temperature and gives rise to an anomalous electron scattering. A first-order phase transition probably associated with the rattlers is observed at T_p = 7.5 K, below which the mean free path of quasiparticles are enhanced significantly. The reason why such a large electron-phonon coupling is realized in this compound may be found in the structural and electronic duality. KOs_2O_6 presents a unique playground for superconductivity in the sense that an electron-rattler coupling can mediate Cooper pairing in the extremely strong-coupling regime.

ACKNOWLEDGMENTS

We wish to thank M. Takigawa, T. Shibauchi, Y. Matsuda, and H. Harima for fruitful discussions. This research was supported by a Grant-in-Aid for Scientific Research B (16340101) provided by the Ministry of Education, Culture, Sports, Science and Technology, Japan.

[1] M. Hanawa, Y. Muraoka, T. Tayama, T. Sakakibara, J. Yamaura, and Z. Hiroi, Phys. Rev. Lett. **87**, 187001 (2001).

[2] H. Sakai, K. Yoshimura, H. Ohno, H. Kato, S. Kambe, R. E. Walstedt, T. D. Matsuda, Y. Haga, and Y. Onuki, J. Phys.: Condens. Matter **13**, L785 (2001).

[3] R. Jin, J. He, S. McCall, C. S. Alexander, F. Drymiotis, and D. Mandrus, Phys. Rev. B **64**, 180503(R) (2001).

[4] S. Yonezawa, Y. Muraoka, and Z. Hiroi, J. Phys. Soc. Jpn. **73**, 1655 (2004).

[5] S. Yonezawa, Y. Muraoka, Y. Matsushita, and Z. Hiroi, J. Phys. Soc. Jpn **73**, 819 (2004).

[6] S. M. Kazakov, N. D. Zhigadlo, M. Brühwiler, B. Batlogg, and J. Karpinski, Supercond. Sci. Technol. **17**, 1169 (2004).

[7] M. Brühwiler, S. M. Kazakov, N. D. Zhigadlo, J. Karpinski, and B. Batlogg, Phys. Rev. B **70**, 020503(R) (2004).

[8] S. Yonezawa, Y. Muraoka, Y. Matsushita, and Z. Hiroi, J. Phys.: Condens. Matter **16**, L9 (2004).

[9] For KOs_2O_6, Yamaura *et al.* reported the space group *Fd*-3*m* in their single-crystal X-ray diffraction (XRD) experiments [J. Yamaura, S. Yonezawa, Y. Muraoka, and Z. Hiroi, J. Solid State Chem. 179, 336 (2005)], while, recently, Schuck *et al.* claimed a different space group of *F*-43*m* that lacks inversion symmetry in their XRD study at room temperature [G. Schuck, S. M. Kazakov, K. Rogacki, N. D. Zhigadlo, and J. Karpinski, Phys. Rev. B 73, 144506 (2006)]. We carefully reexamined the crystal structure using a high-quality crystal and come to a conclusion that *Fd*-3*m* is the most probable space group for KOs_2O_6 at room temperature as well as at low temperatures below T_p, in spite that we observed some forbidden reflections due to double diffractions. We also confirmed this result by using the convergent beam electron diffraction and Raman scattering techniques that are known to sensitive to the symmetry of a crystal.

[10] J. Yamaura, S. Yonezawa, Y. Muraoka, and Z. Hiroi, J. Solid State Chem. **179**, 336 (2005).

[11] V. Keppens, D. Mandrus, B. C. Sales, B. C. Chakoumakos, P. Dai, R. Coldea, M. B. Maple, D. A. Gajewski, E. J. Freeman, and S. Bennington, Nature **395**, 876 (1998).

[12] G. S. Nolas, J. L. Cohn, G. A. Slack, and S. B. Schujman, Appl. Phys. Lett. **73**, 178 (1998).

[13] Z. Hiroi, S. Yonezawa, T. Muramatsu, J. Yamaura, and Y. Muraoka, J. Phys. Soc. Jpn. **74**, 1255 (2005).

[14] M. Brühwiler, S. M. Kazakov, J. Karpinski, and B. Batlogg, Phys. Rev. B **73**, 094518 (2006).

[15] R. Galati, R. W. Hughes, C. S. Knee, P. F. Henry, and M. T. Weller, J. Mater. Chem. **17**, 160 (2007).

[16] J. Kunes, T. Jeong, and W. E. Pickett, Phys. Rev. B **70**, 174510 (2004).

[17] H. Harima, J. Phys. Chem. Solids **63**, 1035 (2002).

[18] D. J. Singh, P. Blaha, K. Schwarz, and J. O. Sofo, Phys. Rev. B **65**, 155109 (2002).

[19] R. Saniz, J. E. Medvedeva, L. H. Ye, T. Shishidou, and A. J. Freeman, Phys. Rev. B **70**, 100505(R) (2004).

[20] R. Saniz and A. J. Freeman, Phys. Rev. B **72**, 024522 (2005).

[21] A. W. Sleight, J. L. Gilson, J. F. Weiher, and W. Bindloss, Solid State Commun. **14**, 357 (1974).

[22] D. Mandrus, J. R. Thompson, R. Gaal, L. Forro, J. C. Bryan, B. C.

Chakoumakos, L. M. Woods, B. C. Sales, R. S. Fishman, and V. Keppens, Phys. Rev. B **63**, 195104 (2001).

[23]Z. Hiroi and M. Hanawa, J. Phys. Chem. Solids **63**, 1021 (2002).

[24]O. Vyaselev, K. Kobayashi, K. Arai, J. Yamazaki, K. Kodama, M. Takigawa, M. Hanawa, and Z. Hiroi, J. Phys. Chem. Solids **63**, 1031 (2002).

[25]Z. Hiroi, J. Yamaura, S. Yonezawa, and H. Harima, to be published in the Proceedings of M2S-2006.

[26]Z. Hiroi, T. Yamauchi, T. Yamada, M. Hanawa, Y. Ohishi, O. Shimomura, M. Abliz, M. Hedo, and Y. Uwatoko, J. Phys. Soc. Jpn. **71**, 1553 (2002).

[27]T. Muramatsu, S. Yonezawa, Y. Muraoka, and Z. Hiroi, J. Phys. Soc. Jpn. **73**, 2912 (2004).

[28]T. Muramatsu, N. Takeshita, C. Terakura, H. Takagi, Y. Tokura, S. Yonezawa, Y. Muraoka, and Z. Hiroi, Phys. Rev. Lett. **95**, 167004 (2005).

[29]R. Khasanov, D. G. Eshchenko, J. Karpinski, S. M. Kazakov, N. D. Zhigadlo, R. Brutsch, D. Gavillet, D. DiCastro, A. Shengelaya, F. LaMattina, A. Maisuradze, C. Baines, and H. Keller, Phys. Rev. Lett. **93**, 157004 (2004).

[30]K. Magishi, J. L. Gavilano, B. Pedrini, J. Hinderer, M. Weller, H. R. Ott, S. M. Kazakov, and J. Karpinski, Phys. Rev. B **71**, 24524 (2005).

[31]R. Khasanov, D. G. Eshchenko, D. DiCastro, A. Shengelaya, F. LaMattina, A. Maisuradze, C. Baines, H. Luetkens, J. Karpinski, S. M. Kazakov, and H. Keller, Phys. Rev. B **72**, 104504 (2005).

[32]K. Arai, J. Kikuchi, K. Kodama, M. Takigawa, S. Yonezawa, Y. Muraoka, and Z. Hiroi, Physica B **359-361**, 488 (2005).

[33]M. Yoshida, K. Arai, R. Kaido, M. Takigawa, S. Yonezawa, Y. Muraoka, and Z. Hiroi, cond-mat/0610760.

[34]Y. Kasahara, Y. Shimono, T. Shibauchi, Y. Matsuda, S. Yonezawa, Y. Muraoka, and Z. Hiroi, Phys. Rev. Lett. **96**, 247004 (2006).

[35]Shimojima and S. Shin, private communications (2006).

[36]A. Koda, W. Higemoto, K. Ohishi, S. R. Saha, R. Kadono, S. Yonezawa, Y. Muraoka, and Z. Hiroi, J. Phys. Soc. Jpn. **74**, 1678 (2005).

[37]Z. Hiroi, S. Yonezawa, J. Yamaura, T. Muramatsu, and Y. Muraoka, J. Phys. Soc. Jpn. **74**, 1682 (2005).

[38]Z. Hiroi, S. Yonezawa, and J. Yamaura, J. Phys.: Condens. Matter **19**, 145283 (2007).

[39]Z. Hiroi and S. Yonezawa, J. Phys. Soc. Jpn. **75**, 043701 (2006).

[40]B. Darriet, M. Rat, J. Galy, and P. Hagenmüller, Mat. Res. Bull. **6**, 1305 (1971).

[41]D. W. Murphy, R. J. Cava, K. Rhyne, R. S. Roth, A. Santoro, S. M. Zahurak, and J. L. Dye, Solid State Ionics **18&19**, 799 (1986).

[42]E. Ohmichi, T. Osada, S. Yonezawa, Y. Muraoka, and Z. Hiroi, J. Phys. Soc. Jpn. **75**, 045002 (2006).

[43]T. Shibauchi, L. Krusin-Elbaum, Y. Kasahara, Y. Shimono, Y. Matsuda, R. McDonald, C. H. Mielke, S. Yonezawa, Z. Hiroi, M. Arai, T. Kita, G. Blatter, and M. Sigrist, Phys. Rev. B **74**, 220506(R) (2006).

[44]J. P. Carbotte, Rev. Mod. Phys. **62**, 1027 (1990).

[45]H. Padamsee, J. E. Neighbor, and C. A. Shiffman, J. Low Temp. Phys. **12**, 384 (1973).

[46]F. Bouquet, Y. Wang, R. A. Fisher, D. G. Hinks, J. D. Jorgensen, A. Junod, and N. E. Phillips, Europhys. Lett. **56**, 856 (2001).

[47]V. Guritanu, W. Goldacker, F. Bouquet, Y. Wang, R. Lortz, G. Goll, and A. Junod, Phys. Rev. B **70**, 184526 (2004).

[48]M. Nohara, M. Isshiki, F. Sakai, and H. Takagi, J. Phys. Soc. Jpn. **68**, 1078 (1999).

[49]A. L. Fetter and P. C. Hohenberg, in *Superconductivity*, edited by R. D. Parks (M. Dekker, New York, 1969), p. 817.

[50]T. McConville and B. Serin, Phys. Rev. **140**, A1169 (1965).

[51]S. Paschen, W. Carrillo-Cabrera, A. Bentien, V. H. Tran, M. Baenitz, Y. Grin, and F. Steglich, Phys. Rev. B **64**, 214404 (2001).

[52]Z. Hiroi, M. Hanawa, Y. Muraoka, and H. Harima, J. Phys. Soc. Jpn. **72**, 21 (2003).

[53]G. W. Webb, Z. Fisk, J. J. engelhardt, and S. D. Bader, Phys. Rev. B **15**, 2624 (1977).

[54]A. P. Mackenzie, R. K. W. Haselwimmer, A. W. Tyler, G. G. Lonzarich, Y. Mori, S. Nishizaki, and Y. Maeno, Phys. Rev. Lett. **80**, 161 (1998).

[55]D. W. Woodard and G. D. Cody, Phys. Rev. **136**, A166 (1964).

[56]Z. Fisk and G. W. Webb, Phys. Rev. Lett. **36**, 1084 (1976).

[57]A. Ioffe and A. R. Regel, Prog. Semicond. **4**, 237 (1960).

[58]P. B. Allen, W. E. Pickett, K. M. Ho, and M. L. Cohen, Phys. Rev. Lett. **40**, 1532 (1978).

[59]H. Wiesmann, M. Gurvitch, H. Lutz, A. Ghosh, B. Schwarz, M. Strongin, P. B. Allen, and J. W. Halley, Phys. Rev. Lett. **38**, 782 (1977).

[60]O. Vyaselev, K. Arai, K. Kobayashi, J. Yamazaki, K. Kodama, M. Takigawa, M. Hanawa, and Z. Hiroi, Phys. Rev. Lett. **89**, 017001 (2002).

[61]M. Furuyama, N. Kobayashi, and Y. Muto, Phys. Rev. B **40**, 4344 (1989).

[62]P. B. Allen and R. C. Dynes, Phys. Rev. B **12**, 905 (1975).

[63]L. R. Testardi, Rev. Mod. Phys. **47**, 637 (1975).

[64]S. D. Bader, G. S. Knapp, S. K. Sinha, P. Schweiss, and B. Renker, Phys. Rev. Lett. **37**, 344 (1976).

[65]S. Sanada, Y. Aoki, A. Tsuchiya, D. Kikuchi, H. Sugawara, and H. Sato, J. Phys. Soc. Jpn. **74**, 246 (2005).

[66]K. Hattori, Y. Hirayama, and K. Miyake, J. Phys. Soc. Jpn. **74**, 3306 (2005).

[67]J. Yamaura and Z. Hiroi, in preparation.

[68]M. Tinkham, *Introduction to superconductivity* (Dover Publications, inc., New York, 1996).